journal of the international meteor organization

WGN

45:4
august 2017

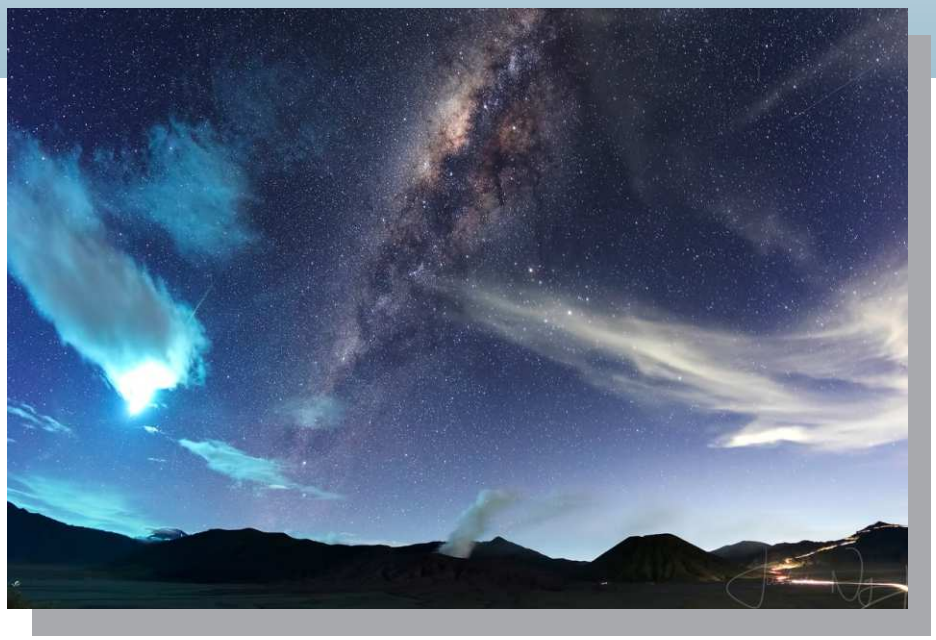

New radio meteor detecting and logging software
Temporal and spatial variation of meteor flux in radio data
February–March video meteors

ISSN 1016-3115

WGN Vol. 45, No. 4, August 2017, pp. 67 – 90

Radio meteors

New radio meteor detecting and logging software *Wolfgang Kaufmann* 67

Temporal and Spatial Variation of Meteor Flux in Radio Data *Charles Powell and Kristina Veljković* 73

Preliminary results

Results of the IMO Video Meteor Network — February 2017 *Sirko Molau, Stefano Crivello, Rui Goncalves, Carlos Saraiva, Enrico Stomeo, and Javor Kac* 82

Results of the IMO Video Meteor Network — March 2017 *Sirko Molau, Stefano Crivello, Rui Goncalves, Carlos Saraiva, Enrico Stomeo, and Javor Kac* 87

Front cover photo

Brilliant Eta Aquariid, captured from Mount Bromo, Indonesia on 2017 May 6 at around $04^{\mathrm{h}}16^{\mathrm{m}}$ AM local time. Evolution of the persistent train is presented on the back cover. Photo courtesy: Justin Ng.

Writing for WGN

This Journal welcomes papers submitted for publication. All papers are reviewed for scientific content, and edited for English and style. Instructions for authors can be found in WGN **45:1**, 1–5, and at `http://www.imo.net/docs/writingforwgn.pdf` .

Legal address

International Meteor Organization, Jozef Mattheessensstraat 60, 2540 Hove, Belgium.

Radio meteors

New radio meteor detecting and logging software

Wolfgang Kaufmann[1]

A new piece of software "Meteor Logger" for the radio observation of meteors is described. It analyses an incoming audio stream in the frequency domain to detect a radio meteor signal on the basis of its signature, instead of applying an amplitude threshold. For that reason the distribution of the three frequencies with the highest spectral power are considered over the time (3f method). An auto notch algorithm is developed to prevent the radio meteor signal detection from being jammed by a present interference line. The results of an exemplary logging session are discussed.

Received 2017 June 7

1 Introduction

Meteor observation by forward scattering of radio waves off meteor trails is well established. This technique mostly uses the audio output of an appropriate receiver (Rendtel & Arlt, 2015). Detecting and logging of the meteor signals in the audio stream can be done by a computer with suitable software. Different software solutions exist for this purpose. Gathering hourly count rates with arbitrary methods may not contribute much to scientific progress but give an instantaneous result to the meteor enthusiast. On the other hand recording raw data (even of the radio frequency by means of a software defined radio) preserves a lot of information with little methodical bias. Nowadays storage of large amounts of data is no longer expensive but this solution is unattractive to the enthusiast because there is no prompt feedback. Also, a huge amount of data must be processed most of which are of no relevance.

Here a new software package Meteor Logger is described. Its current version is 1.21. It has been developed by the author with the goal to find a solution to the aforementioned dilemma. This software detects signals and records them with a high frequency and temporal resolution. For this purpose, signal detection relies on identifying signal signatures in the frequency domain instead of using an amplitude threshold. A tabular on-screen output of detected meteor signals gives immediate feedback. For further processing the data are also written to disc. These data allow studying Doppler shift of head echoes as well as compiling power profiles. Hourly count rates can be extracted. Because many meteor enthusiasts live in populated areas polluted by man-made noise a measure is implemented to partly overcome interference. The program is free software under the GNU General Public License and is based on Python 3. It can be downloaded from the author's website at:
`http://www.ars-electromagnetica.de/robs/download.html`.

2 Material and Methods

All analysis for the development of Meteor Logger and all testing was performed on radio signals reflected from the radar beam at 143.050 MHz from GRAVES, France. The location was Algermissen, Northern Germany (N 52°15′16, E 009°58′71). A HB9CV-antenna was directed to the transmitter location and fed to a FUNcube Dongle Pro+ (FCDP). The FCDP[a] is a software defined receiver. This means all filtering and demodulation is done by software. SDR# was used as receiving software[b]. For its cooperation with Meteor Logger it was set to USB, 143.049 MHz receiving frequency, 48 kHz audio output, audio filtering and AGC switched off. Both programs ran on the same computer (Intel i5, clock speed 2.3 GHz) with Windows 7. The FCDP has not been frequency calibrated, so the received audio signals from meteor trails must not be expected at 1000 Hz exactly. For comparison also the spectrum analyzer software Spectrum Lab from Wolfgang Büscher, DL4YHF[c] was used with a conditional action script that performs a threshold-based signal registration[d].

3 Principle of function

Meteor Logger continuously takes overlapping chunks of data from the audio stream of the sound-card. Each chunk includes 2048 samples. Overlap amounts to 75 percent. With a sample rate of 48 kHz this results in a frequency resolution of 23.4 Hz, a time frame of 43.7 ms and a temporal resolution of 10.7 ms. This configuration is derived empirically from the study of high resolution spectra of prerecorded meteor signals from GRAVES. A Blackmann-Harris window function is applied to the samples of each chunk. Then a Fast Fourier Transformation (FFT) is performed to get the frequency spectrum of each chunk. Figure 1 gives an example of such a time sliced meteor signal. Adjustable frequency limiters narrow the FFT-spectrum down for the following analysis.

Meteor Logger pursues the goal not to use an amplitude threshold for detecting radio signals of me-

[1]Lindenweg 1e, 31191 Algermissen, Germany.
Email: `contact@ars-electromagnetica.de`

IMO bibcode WGN-454-kaufmann-meteorlogger
NASA-ADS bibcode 2017JIMO...45...67K

[a] `http://www.funcubedongle.com/`
[b] `http://airspy.com/download/`
[c] `http://www.qsl.net/dl4yhf/spectra1.html`
[d] `http://www.ars-electromagnetica.de/robs/index.html`

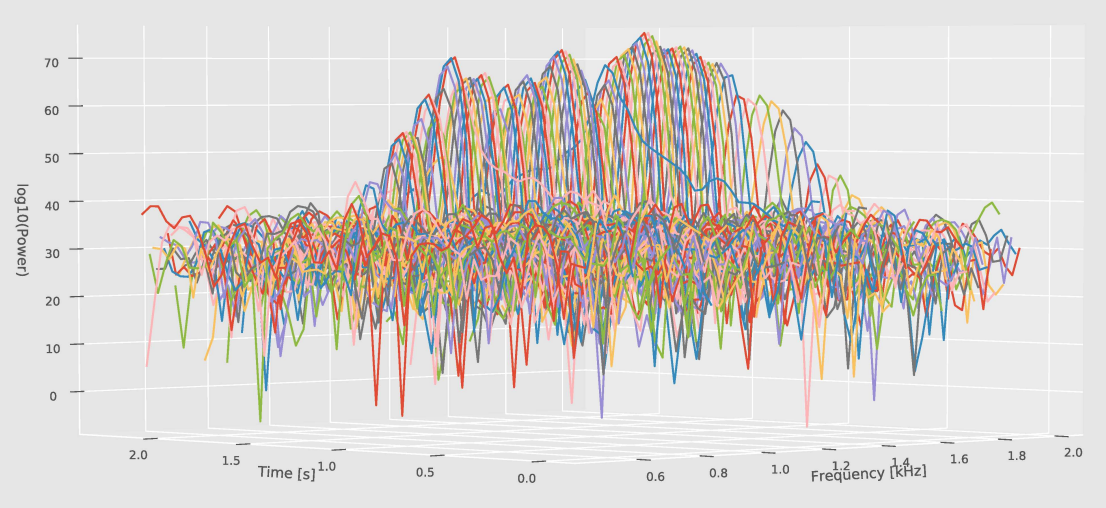

Figure 1 – A 3D-Plot of a meteor signal as outcome of a series of subsequent FFTs. The logarithm of spectral power of the audio signal (arbitrary units) is plotted against time in s and frequency in kHz. As can be seen the meteor signal stands out as small ridge from surrounding noise. (The software for this analysis was written by the author).

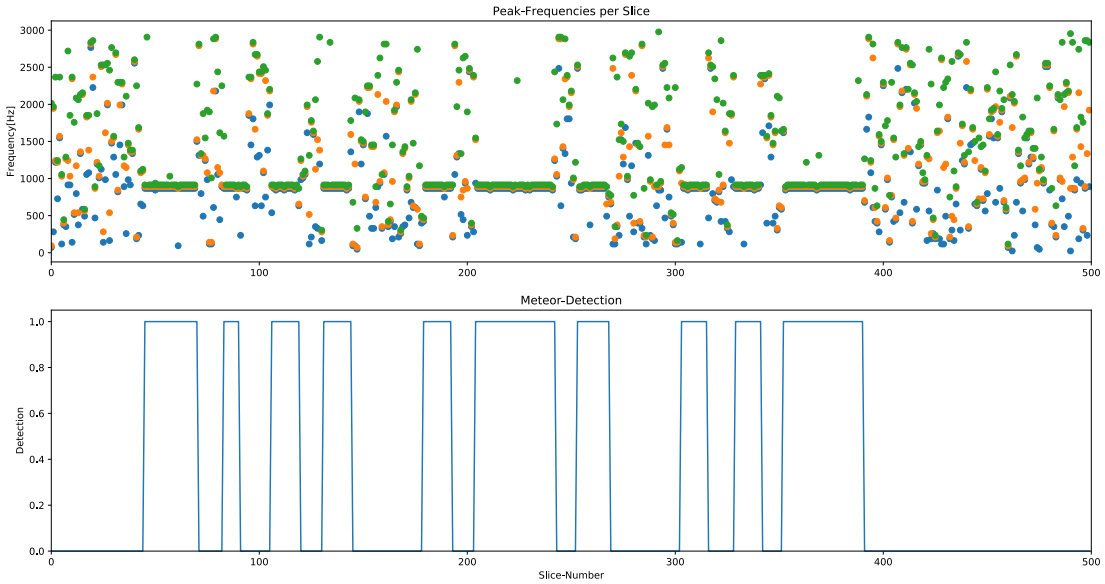

Figure 2 – Image of the diagnostic screen of Meteor Logger. The upper graph shows the distribution of the three frequencies with the highest power (3f) within the selected bandwidth 0 – 3000 Hz of each FFT. A cw-transmission is used for demonstration. At the presence of a signal, the random dispersion of the 3f is lost and the 3f agglomerate around the signals peak frequency. The lower graph shows the result of the detecting algorithm.

teors but act on the detection of signal signatures. The basic idea is to extract the three frequencies with the highest power (3f) within the FFT. At the presence of white noise, these 3f are randomly distributed over the spectral range of the FFT. The more a signal stands out from noise the more the 3f concentrate around the signal's peak frequency (see Figure 2). So the first step is to detect such an agglomeration and determine its peak frequency (pf). This agglomeration also happens irregularly at the presence of noise, so further criteria have to be applied to isolate a real signal. Therefore in an additional step it is checked whether the pf emerge in subsequent FFTs in a special manner: a pf must not deviate more than 117 Hz from its predecessor. This accounts for a maximum Doppler shift of 11 kHz/s for head echoes. From testing with white noise at a bandwidth of 2.5 kHz a series of 5 / 6 FFTs are found to be suitable, resulting in 1.5 / 0.7 erroneous signal registrations per hour respectively. Thereby one gap is allowed at random position within each series (indicated by setting the frequency-record to −1). These lengths of series are implemented as sensitive / robust detection mode. Hence a meteor signal must be present 40 / 50 ms at minimum to be registered.

The 3f-method requires a continuous wave transmitter to work properly. An AM transmission may function because the carrier is much more powerful than the side-bands are. Meteor Logger should lock on the carrier. Any multi-frequency transmissions like FM or the countless digital modes will not operate.

Meteor Logger logs date, local time, peak-frequency, the power at the peak-frequency and the

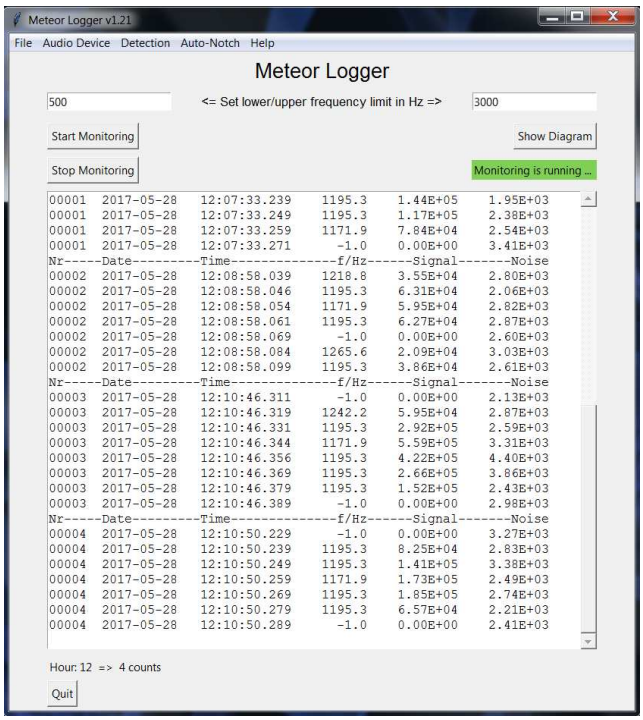

Figure 3 – A screenshot of the GUI of Meteor Logger. The actual log is displayed and also the raw counts/h. This allows one to follow the actual meteor activity as well as to control interference situation.

power of the noise of each chunk only during signal detection. A serial number is assigned to each signal detection. Noise is indicated as the median of the distribution of spectral power within the selected frequency limits. Within noisy surroundings it can be used for corrections. Time is taken from the system clock immediately after a chunk is taken from the audio stream. The log is displayed in real time in a window of Meteor Logger's GUI (see Figure 3) and also on disc as `.csv` file.

Against persistent interference an auto-notch algorithm is implemented. It drastically reduces the power at the frequency rated as interference before the signal detection takes place, so a meteor signal detection is possible despite the presence of interference. Determining a signal as interference is based on the persistence of agglomerated 3f with a common pf. A common pf is assumed if the standard deviation of an adjustable number of consecutive pfs (Meteor Logger's auto-notch speed option) drops below a predefined threshold. This threshold can not be a fixed value because the standard deviation depends on the range of frequencies chosen as analysis bandwidth. Three quadratic equations with different coefficients for three degrees of responsivity (Meteor Logger's auto-notch responsivity option) are adopted to determine the threshold as a function of the analysis bandwidth. If the condition is fulfilled, the pf will be regarded as interference and its power will be reduced.

4 Results

The logging session of Meteor Logger presented here shall only demonstrate its capabilities and also its shortcomings. It took place from 2017 May 20, $15^{h}00^{m}$ local time CEST (CEST = UTC + 2^{h}) to May 21, $14^{h}59^{m}$. It was performed with robust mode, auto-notch speed slow, auto-notch responsivity high and frequency limits set to 400 and 2900 Hz respectively. The graph of the registered frequencies gives an overview of the session (see Figure 4). Each dot represents the peak-frequency of one FFT of a detected signal. The largest number of dots originate from meteor trails exhibiting only small Doppler shift by high winds. They are centered around 1195 Hz. Zooming into the data to a deep fading overdense meteor (see Figure 5) shows that Meteor Logger registers this single meteor event as three separate signals. So for extracting hourly count rates, a time lapse must be defined and applied to conflate such signals. This is also true for determining the duration of the meteors.

Figure 4 also exhibits some impressive Doppler-shifted head echoes. Zooming into the data of such a meteor results in Figure 6. Graph (A) displays the devolution of frequency and graph (B) exhibits the power profile as signal to noise ratio (SNR) of the selected meteor. SNR is given in decibels, a logarithmic measure that is ideal for depicting the very high dynamic range of the meteor signal. The power profile has a high spectral purity with a bandwidth of 23.4 Hz.

There are at least a couple of non-meteor signal registrations present (false positives). The most evident are marked with an ellipse in Figure 4. They have different origins. Some are simply detection errors as described above. The very elongated ellipses mark satellite passes and an aircraft transit. The intermittent structure of these signals is based on how GRAVES is operated (somewhat like a lighthouse with four rotating beams, see `http://dk5ec.de/Graves-Echo-english.pdf`). Most false positives have their origin in man-made noise: during the logging session the waterfall spectrogram of SDR# showed drifting noise bands of irregular shape and pulsating harmonics with a bandwidth of 1–2 kHz. However broadband noise (ignition sparks, lightning) and interference lines with a bandwidth less than 25 Hz did not affect Meteor Logger. Table 1 gives a quantitative overview. Most false positives can be identified on the basis of their frequency and power, but some false positives come with a frequency close to the frequencies of the meteor trails and a similar power. These remain unidentified. In the case of false positives having an equal frequency distribution over the bandwidth their number can easily be estimated: The ratio of the frequency segment around the frequencies of the meteor trails to the bandwidth reveals the fraction of unidentified false positives. Its multiplication with the total number of identified false positives results in the number of unidentified false positives.

Interference has to be removed prior to obtain the correct hourly count rate. Fading signals must be conflated and for purpose of standardisation an amplitude threshold has to be applied. The result (here without applying an amplitude threshold) is shown in Figure 7. Starting with declining count rates a minimum of about 20 counts/h is reached at 19^{h} CEST. From then on the

Table 1 – Signal identification of the 24 h logging session. The identification of false positives bases on frequency and power. Some false positives may have the a frequency close to the frequencies of meteor trails and a similar power and thus remain unidentified. They are estimated assuming an equal frequency distribution of the false positives. Thereby five times the frequency resolution is considered the relevant frequency segment (see text for calculation).

	Identified false positives	Estimated false positives	Meteor signals
Detection errors	15		
Man-made interference incl. aircraft- and satellite-transits	91		
Total	106	5	1388

hourly count rates are rising slowly to gain about 70 counts/h between 04^h and 08^h. An outstanding maximum is seen from 09^h to 10^h CEST. This may be assigned to the meteoroids of the o-Cetids (293 DCE). This shower was predicted to have a peak at 2017 May 20, 09^h UTC (Rendtel, 2016).

Auto notch works fine with a persistent interference of small bandwidth (see Figure 8). However Auto-notch cannot cope with intermittent interference.

5 Discussion

Comparing Meteor Logger to Spectrum Lab, almost the same hourly count rates can be found after processing the raw data of each session appropriately. This is a strong indication for the proper working of Meteor Logger. Selecting the sensitive mode of Meteor Logger an even enhanced responsivity can be achieved at the expense of a higher susceptibility to interference and erroneous registrations due to noise. The specified parameters of sample rate, temporal and frequency resolution together with the algorithm for detecting signals are well equipped to deliver reliable results at least in relation to GRAVES radar.

Because of the applied 3f-method, noise is a major theme to Meteor Logger. As long as noise is broadband, Meteor Logger is immune against it. The smaller the frequency distribution of noise becomes, i.e. the more the noise becomes the character of a signal, the more erroneous registrations will occur. Thereby strong interference blocks any registration of weaker signals. At least at an interference bandwidth of less than 100 Hz auto-notch will become effective. An even more narrow bandwidth of interference (less than 25 Hz) will be ignored by Meteor Logger because such a small bandwidth cannot agglomerate the 3f (see above). This behavior is different to threshold-based detection systems which respond equally to any interference by adding the power of interference and signal. In this logging session 106 false positives could be identified and removed. An uncertainty of 5 false positives is assumed (Table 1) provided the false positives have an equal frequency distribution. If these are pooled in a small time span particularly the hourly count rate will be biased.

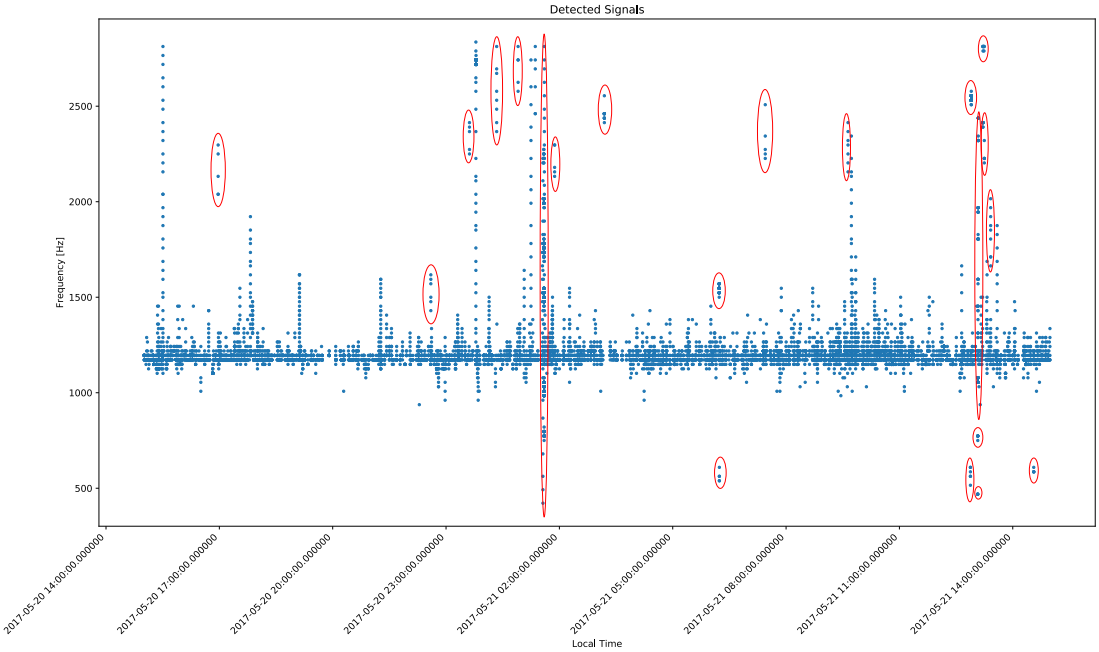

Figure 4 – A frequency vs. time plot of a 24 h logging session. Each dot represents the frequency with the highest power of a FFT being part of a detected signal. Bandwidth is set to 400 – 2900 Hz. Signals evoked by different types of interference are encircled with red ovals. Most dots belong to meteor trails and some nice head echoes can also be seen.

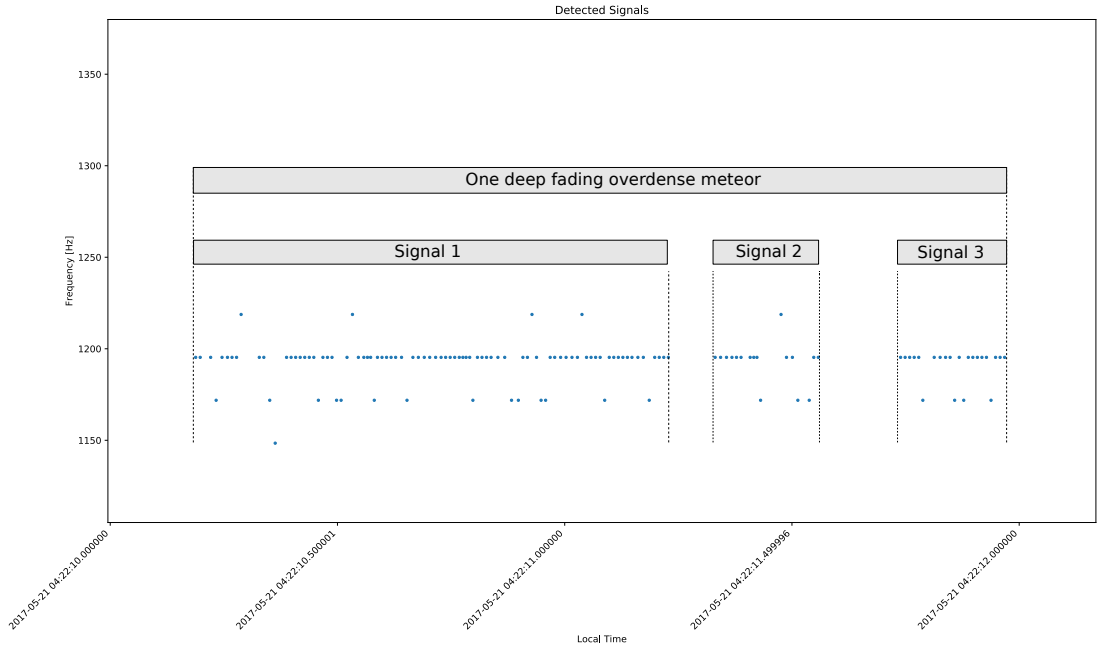

Figure 5 – Zooming into the graph of Figure 4 reveals an overdense meteor trail with deep fading resulting from interference due to secondary reflection points caused by wind shear. Multiple moving reflection points can appear on a trail that is distorted by strong winds in the upper atmosphere (Rendtel & Arlt, 2015). Deep fading causes the detecting algorithm of

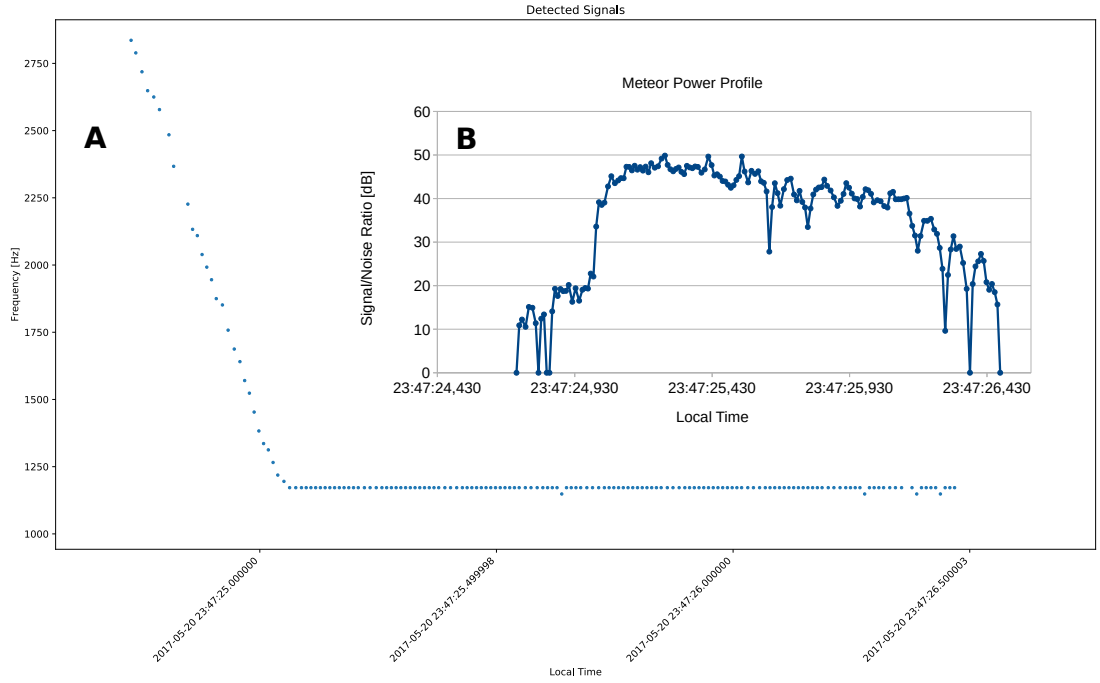

Figure 6 – (A) A deep zoom into the graph of Figure 4 outcrops a complete meteor registration with head echo as well trail reflection. (B) shows the power profile of this meteor as signal to noise ratio to properly depict the huge dynamic range.

Auto-notch works well in the test but it cannot distinguish between persistent interference and long lasting meteor signals. After a certain amount of FFTs with a continuous signal present it starts notching this signal. Therefore a long lasting meteor signal can be truncated. To avoid this the auto-notch speed must be adjusted to the awaited duration of incoming meteor signals or even switched off. An intermittent interference will not trigger the auto-notch function.

The recorded raw data allow for processing to get a corrected and standardised output. Irregularities can be identified and excluded. A software allowing viewing and zooming into the data as well as processing them is in development by the author. Meanwhile a spreadsheet program will do the job.

The precision of timing is mainly an issue of the long-term accuracy of the system clock. Multitasking will also bias the readout of time to a degree that de-

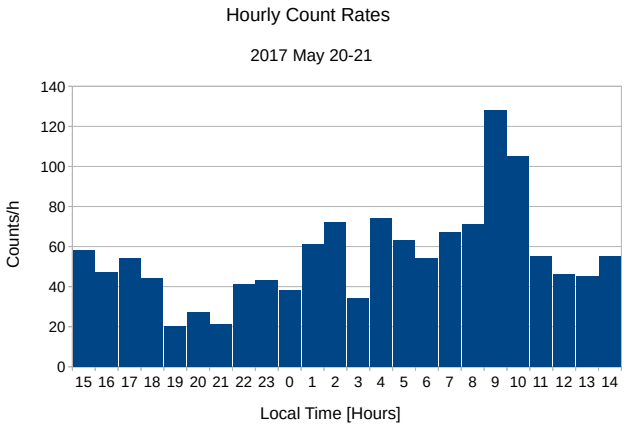

Figure 7 – Hourly count rates after removing identified interference (see Table 1) and conflate distinct signals (see Figure 5). Time is given as CEST. A diurnal variation can be seen as well as a peak at 09^{h}–10^{h} that could be assigned to the o-Cetids.

pends on the computer hardware. If using a SDR the time delay of processing by the SDR-software must be taken into account further. Also Python is an interpreter language. To speed up, the Python script can be transformed in a Cython module.

6 Conclusion

Meteor Logger detects and logs meteor signals with a high frequency and temporal resolution. The detailed log of time, frequency and power of the detected signals allow for a later processing of the recorded events. Interference can be identified and removed. A detailed study of single meteor signals can be performed. Overall measures like hourly count rates or logarithmic cumulative amplitude or duration distributions can be extracted in a standardised way.

Meteor Logger delivers reliable results fully comparable to Spectrum Lab software running an action script for meteor detection.

Meteor Logger reacts differently to interference than threshold-based systems do. It proved to be widely immune against broad-band (white) noise as well as interference lines with a very small bandwidth (< 25 Hz). Otherwise, strong interference blocks the registration of weaker signals completely. However an auto-notch function allows for registering weak signals at least at the presence of persistent interference occupying a bandwidth less than 100 Hz.

The raw data as well as the raw number of counts of the actual hour are displayed on-screen immediately after each detection of a signal.

Meteor Logger requires a continuous wave transmitter to work properly. Any multi-frequency transmissions like FM or digital modes will not operate.

References

Rendtel J. (2016). "2017 Meteor Shower Calendar". IMO INFO (2-16).

Rendtel J. and Arlt R. (2015). *Handbook for Meteor Observers*. International Meteor Organization, Potsdam.

Handling Editor: Javor Kac

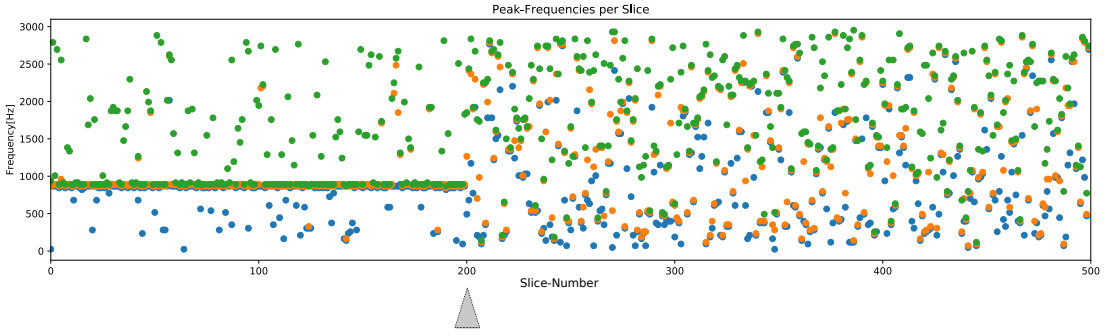

Figure 8 – Image of the diagnostic screen of Meteor Logger showing the distribution of the three frequencies with the highest power (3f) within the selected bandwidth 0 – 3000 Hz of each FFT. An interfering signal is present at about 900 Hz. Auto-notch is activated and starts to eliminate the signal (marked by an arrow).

Temporal and Spatial Variation of Meteor Flux in Radio Data

Charles Powell[1,2,3] *and Kristina Veljković*[4]

The variation of hourly detection counts from almost 350 radio meteor detection stations is analysed to determine the effect of year, time of day, and latitude on observations, as well as discussions of annual and monthly variations. Results indicate a significant increase in hourly detection counts in 2009–2010, supporting previous hypotheses of correlation between radio meteor detection rates and solar activity. Annual increases in meteor rates during summer months are noted, with no clear explanation. Monthly variations are not significant. The effect of latitude on detection counts is significant for years 2005–2016. For 12 of 17 considered years, night-time detection counts are greater than day-time counts, likely due to changes in ionospheric structure at night.

Received 2017 September 6

1 Introduction

Many patterns arise in meteor detection: for example diurnal variations in meteor flux, or meteor showers which cause variation in activity rates. These trends often occur periodically, and studies of temporal variation help to study the mechanisms that cause these trends. In pursuit of this, the variation of radio meteor detection results is analysed over a daily, monthly, and annual scale. Influences of the time of day and latitude are also considered. This analysis is made using a database of hourly detection counts, provided by the Radio Meteor Observation Bulletin (RMOB)[a].

Lindblad (1968) analyses long-term variation in meteor radar rates, as well as echo amplitudes. Echo amplitudes are seen to correlate with electron line density, indicating an influence from the solar wind. It is also observed that long-term variation in radio meteor detection count can be explained qualitatively by a variation in atmospheric electron density in the region where most meteors burn up, which itself is related to the solar cycle.

Bumba (1949) calculates the yearly rate of meteors as a function of the position of the Sun in the solar cycle, demonstrating an inverse relationship between solar activity and detection counts.

Singer et al. (2005) note an increasing diurnal rate with decreasing latitude, suggesting that overall, hourly detection counts increase with lower latitudes. A greater meteor flux in summer (for the Northern Hemisphere) is noted.

2 Method

2.1 Data collection

The data used are from the publicly available collection of observer records provided by the Radio Meteor Observation Bulletin (RMOB). The locations of the observers are spread across the globe. This does not present an issue when considering the data as a whole, since individual observers' variations in data will be insignificant, given a sample size of almost 350. Thus the influence of individual setups is disregarded. Spatial variations may be present: these are considered.

Table 1 – Number of observers by latitude class.

Latitude class (°)	N^o observers
N(45–60)	135
N(30–45)	45
N(15–30)	5
S(15–30)	2
S(30–45)	4

Collection of data from the website was automated using a script. Once obtained as a raw text file, the file was parsed and stored using custom Python objects. 'Observer' objects contain the username, a Python dictionary containing their data, location attributes, and detection setup information for the given observer. The data dictionary was populated with 'Entry' objects, which are a single month of data and contain the date in format YYYY-MM, data source URL, and the data itself. If the same observer reported a different detection setup in a certain month, this was separated into a different object. Some website users used a different username occasionally – these data were combined, provided the detection setup is identical, otherwise placed in a new object.

There were 345 observer objects in total. 213 of these contain both latitude and longitude co-ordinates in decimal degrees. For analysing monthly and annual variation of detection counts, these data were suitably formatted and only required categorising by month or day. For statistical analysis, the data were compiled into a spreadsheet of tuples of detection counts for each hour available, split by latitude class. Longitude classes were not analysed since longitude does not represent a significant effect to be considered. Equally, further splitting the data by longitude as well as latitude would have reduced sample sizes further, making some classes too small to be analysed. Table 1 shows the number of observers by latitude class and period of the day. Note that not all observers with sufficient location data were included, since some do not have enough valid data.

Before being compiled into the spreadsheet, duplicated data were removed, when an observer has entered

[1]Exeter Mathematics School, Exeter, Devon, EX4 3PU, United Kingdom
[2]Norman Lockyer Observatory, Sidmouth, Devon, EX10 0NY, United Kingdom
[3]Email: cpowell@cwp.io
[4]Faculty of Mathematics, University of Belgrade, Studentski trg 16, 11000 Belgrade, Serbia. Email: kristina@matf.bg.ac.rs

IMO bibcode WGN-454-powell-temporal
NASA-ADS bibcode 2017JIMO...45...73P
[a]Accessible at www.rmob.org.

Table 2 – Total number of detection counts and removals by latitude class and period of day.

Latitude class (°)	Day counts	Day removals	Night counts	Night removals
N(45–60)	430 685	22 970	312 143	14 346
N(30–45)	191 336	3 736	177 142	2 970
N(15–30)	4 029	0	3 986	0
S(15–30)	4 781	0	3 426	0
S(30–45)	6 691	157	7 236	175

the same set of data twice onto the RMOB website. Data were split into day or night periods by defining night as 12 hours centred at local midnight. Values greater than 1000 were considered too extreme, and were not included. The value at which counts are considered extreme is arbitrary and of little importance. A threshold of 1000 was chosen as it results in the removal of relatively few counts. In total, for latitude classes, there were 637 552 day-time counts after 26 863 were removed, and 503 933 night-time counts after 17 491 were removed. A full breakdown of counts and removals is given in Table 2.

2.2 Research hypotheses

1. Is the effect of year on detection counts significant (e.g. detection counts significantly differ for different years)? Are the detection counts collected during the years 2009–2010 significantly higher than other detection counts?

2. Do time of day and latitude have a significant effect on detection counts? Are the night-time detection counts significantly higher than day-time detection counts? Are there significant differences in detection counts when going from southern latitudes to northern latitudes?

2.3 Statistical analysis

The distribution of the detection counts collected during the period 2000–2016 was analysed with graphical representation (histogram) and with descriptive statistics (mean, median, first and third quartile, coefficients of skewness and kurtosis). Statistical tests for normality were not used. Because of the large sample size, these tests are very sensitive and would detect extremely small departures from a normal distribution.

Fligner-Killen test of homogeneity of variances (Conover et al., 1981) was used to examine if the variability of detection counts collected during the period 2000–2016 is approximately the same. Significance of the effect of year on detection counts was tested by Brunner-Dette-Munk non-parametric one-way ANOVA (Brunner et al., 1997). For examining the effects of period of the day and latitude class on detection counts, Brunner-Dette-Munk non-parametric two-way ANOVA was used. More details about these statistical methods can be found in Rand Wilcox's book (Wilcox, 2012) and complementary R code on his web page (Wilcox, 2016).

Multiple comparisons between detection counts for pairs of years, day-night period of the day, as well as pairs of latitude classes were performed using Brunner-Munzel test (Brunner & Munzel, 2000). The probability of type I error was controlled using Rom's method. Comparisons between two groups were made only if the sample size of the bigger group was at most 100 times greater than the sample size of the smaller group.

P-values < 0.05 were considered statistically significant. Statistical analysis was performed in statistical software R, version 3.4.1 (using packages *e1071*, *lawstat*).

2.4 Monthly & annual variation

In lieu of the statistical analysis, mean ranks were used to analyse variation because the data is asymmetric, so mean is not a good measure of location. Group variances are also not the same, so the data can not be meaningfully compared using median, leaving mean rank as a suitable option. These mean ranks of hourly detection counts for all observers were analysed over monthly and annual timescales, demonstrating the variation of observations in the period 2000–2016.

The hourly detection counts were sorted in increasing order and then ranked. For annual variation of detection counts, the mean rank for each month was calculated by dividing the sum of the ranks of detection counts in that month with total number of monthly counts. Similarly, for monthly variation of detection counts, the mean rank for every day of the month was calculated by dividing the sum of the ranks for that day with the total number of daily counts for that month.

3 Results

3.1 Annual scale variation

The annual variation is shown in Figure 1. The highest mean rank occurs in June. From January to March, there is a decrease in mean rank, followed by a steep increase until June. After this, mean rank steeply decreases until September, with a smaller increase to November, followed by another smaller decrease to December.

3.2 Monthly scale variation

The variation over the course of a month is shown in Figure 2. The variation of mean ranks over the month is small, with no significant increases or decreases except at the beginning of January, the middle of August and the middle of December.

Note that the mean ranks of detection counts for each day of the month are calculated using data from the entire period 2000–2016, so the decrease on the 29th of February occurs due to leap years.

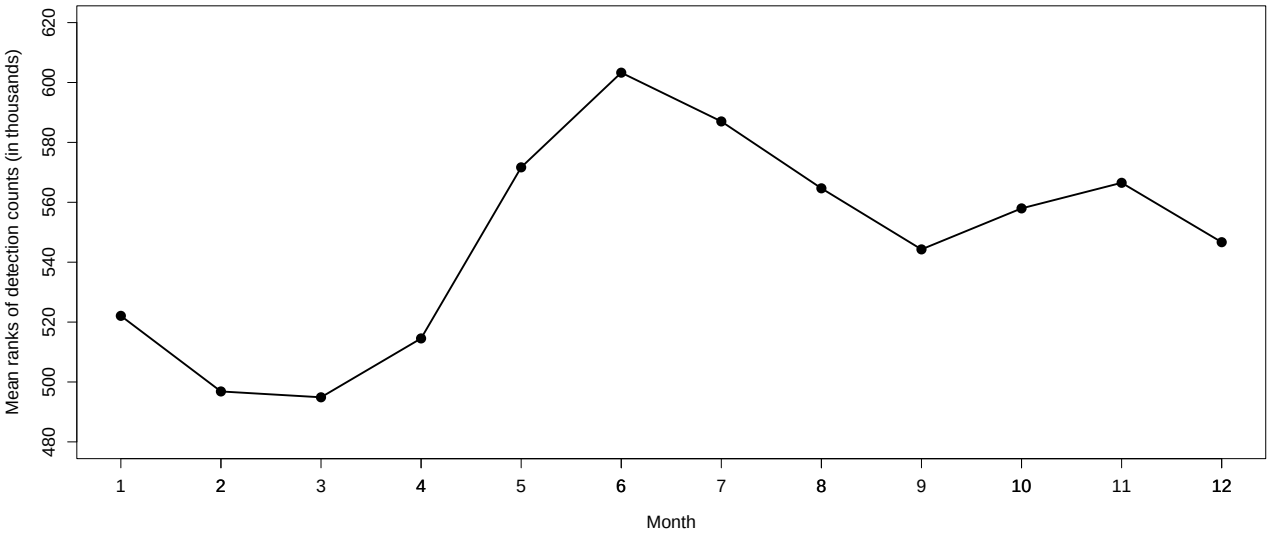

Figure 1 – Variation in mean rank for each month of hourly detection counts collected during the period 2000–2016.

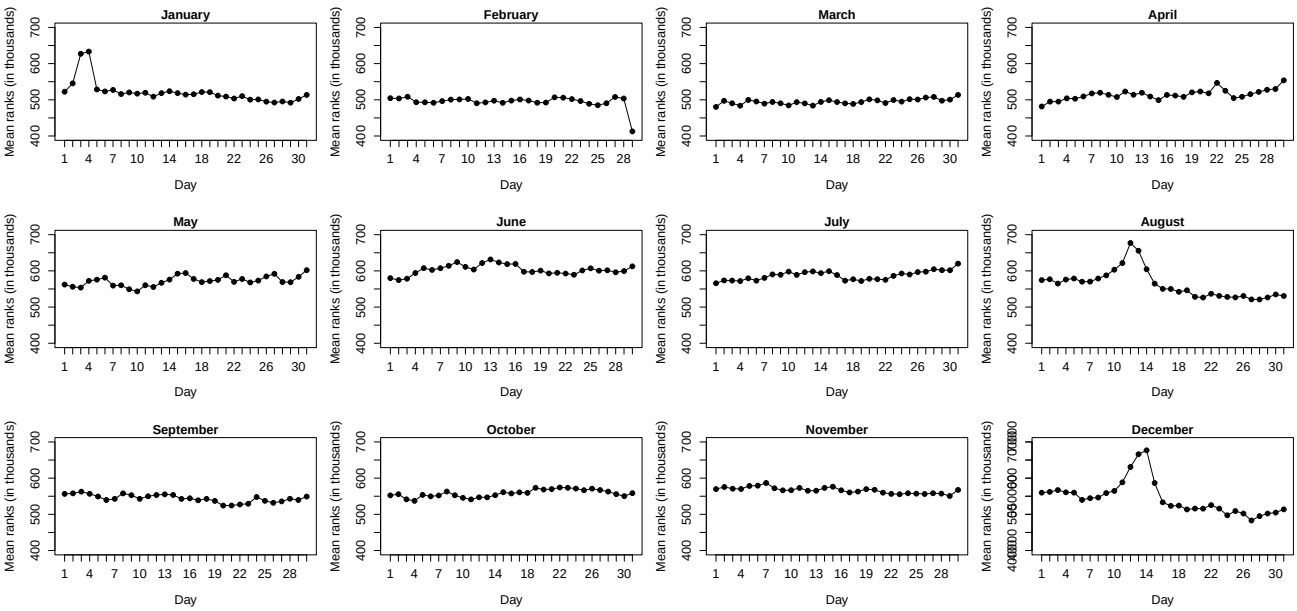

Figure 2 – Variation in mean ranks for each day of each month of hourly detection counts collected during the period 2000–2016.

3.3 Statistical analysis

After removing duplicates and extreme values from the data-set of detection counts, 1 097 101 counts are left. The minimum value of detection counts is 0, and the maximum value is 996. The sample median is equal to 30 and the sample mean to 55.7. The first sample quartile equals 12 and the third is 75. The sample coefficient of skewness is equal to 2.7 and the sample kurtosis, 11.5. The normal distribution has coefficient of skewness equal to 0 and coefficient of kurtosis equal to 3. Values of skewness and kurtosis of detection counts suggest a distribution that is skewed to the right (positively skewed), with higher peak and longer tail than a normal distribution. Detection counts are represented as a histogram in Figure 3. The bins of the histogram are of length 10. In the first bin (0–10 counts) there are 244 364 detections. Starting from the 421–430 bin, frequencies corresponding to the bins are smaller than 302 and can not be seen on the histogram (zero line). In Figure 3, only counts 0–450 are presented.

We will now inspect whether the variability of detection counts during the period 2000–2016 are approximately the same. Using the Fligner-Killeen test of homogeneity of variances ($\chi^2 = 62\,952$, $df = 16$, $p < 0.001$), we can conclude that year variabilities are not the same (in other words, heteroscedasticity of detection counts by year).

As the distribution of the detection counts is very skewed, in testing our research hypotheses, we could not use standard parametric tests. In the case of heteroscedastic data, even median is not a good choice for the measure of comparisons of different groups. Rather,

Table 3 – Summary statistics of detection counts by year.

Year	Number	Min	Max	1.quartile	Median	3.quartile	Mean rank
2000	8 889	1	996	3	10	35	376 040.5
2001	8 341	1	903	10	18	30	421 829.9
2002	8 710	1	949	9	18	32	399 802.5
2003	7 819	1	532	8	16	31	374 920.3
2004	9 924	1	393	6	11	18	280 121.4
2005	5 763	1	464	5	12	25	314 692.0
2006	5 526	1	334	9	17	30	405 231.9
2007	3 978	1	614	9	21	106	523 092.9
2008	1 230	3	395	19	35	57	575 226.5
2009	25 050	1	995	34	94	169	778 523.5
2010	60 198	1	446	26	53	112	696 070.7
2011	71 985	1	668	18	36	86	604 521.2
2012	136 076	1	905	17	38	83	594 963.6
2013	171 149	1	804	11	29	73	538 737.9
2014	191 108	1	778	11	33	83	560 308.3
2015	193 938	0	818	11	28	73	536 771.0
2016	187 417	0	752	10	22	53	478 370.7

in order to compare distributions of detection counts in different groups, we chose a mean rank. All 1 097 101 detection counts are sorted in increasing order and ranked — the smallest count gets rank 1, second smallest rank 2, and so on, with the largest count getting a value of 1 097 101. Then, the mean rank for each group is calculated (for example the mean rank of detection counts in every year from 2000 to 2016). Group mean ranks are compared in statistical tests. For example, for two groups, a higher mean rank means that there are higher detection counts in that group (though not necessarily a greater maximum detection count).

Summary statistics (number, minimum, maximum, first and third quartile, median and mean rank) of detection counts by year are presented in Table 3.

Mean ranks of detection counts by year are presented in Figure 4. It can be seen that detection counts vary by year. The highest detection counts occurred between 2009 and 2010.

The significance of the effect of year on detection counts is confirmed by Brunner-Dette-Munk nonparametric one-way ANOVA ($F = 2\,158.974$, $df_1 = 6.03$, $df_2 = 12\,429.09$, $p < 0.001$). We will now test the hypothesis that detection counts in 2009 are higher than detection counts in 2010, as well as the hypothesis that detection counts in 2010 are higher than counts in other years. Formally, we first test the existence of difference in detection counts for 2009 and 2010, as the hypothesis is set before seeing the data. The directional hypothesis that detection counts in 2009 are higher than detection counts in 2010 is tested afterwards. Although this can be considered biased, a directional hypothesis is of greater practical significance. Brunner-Munzel test was used for multiple comparisons between two

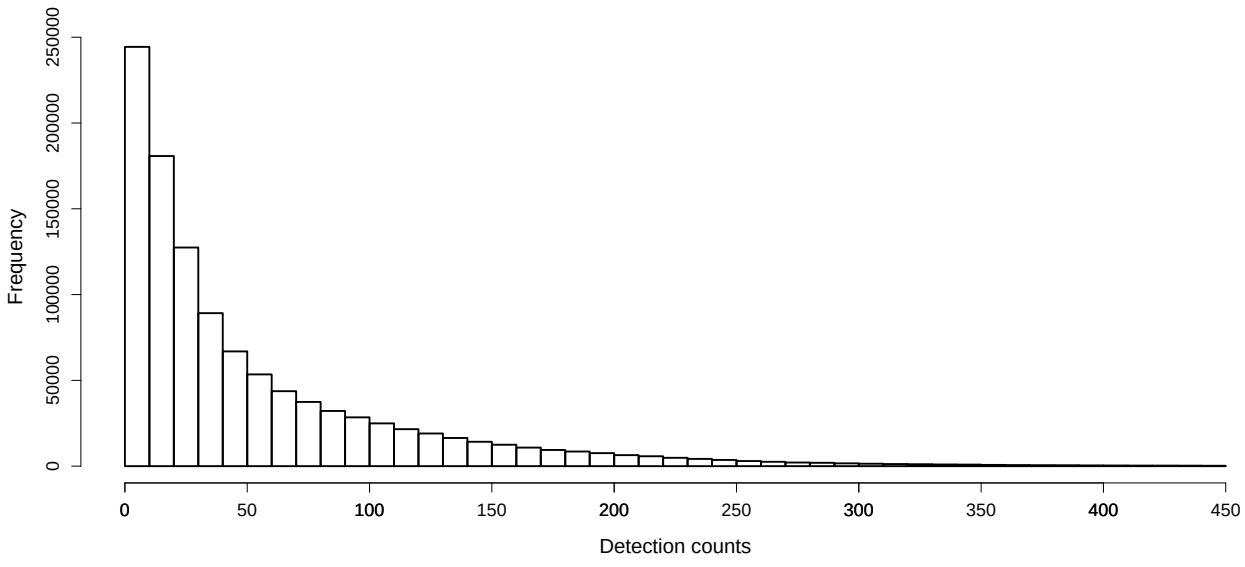

Figure 3 – Histogram of detection counts.

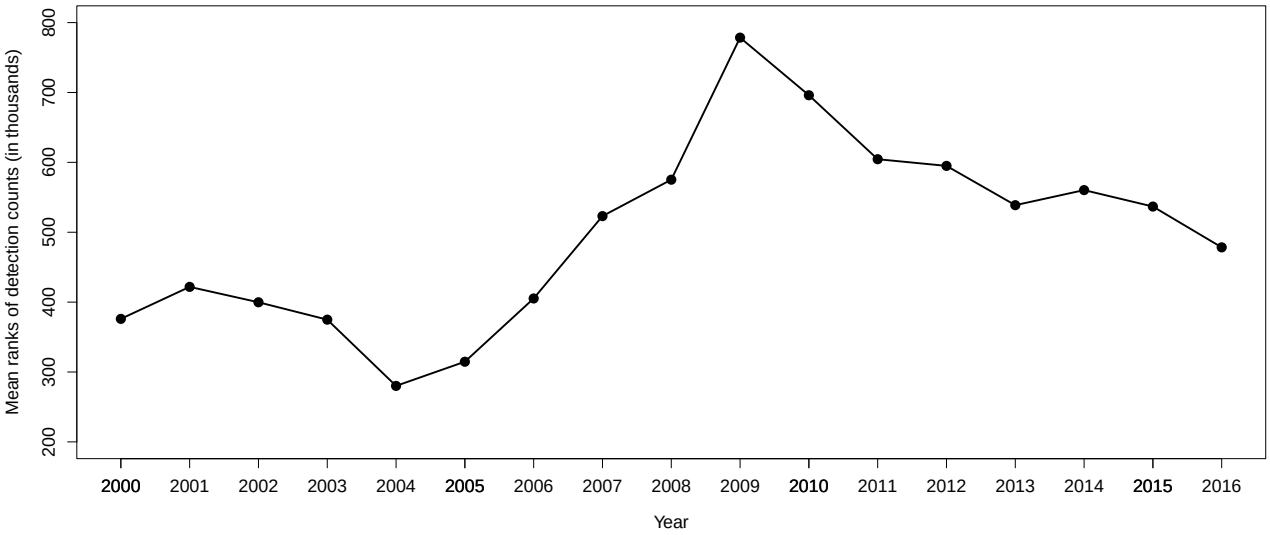

Figure 4 – Plot of mean ranks of detection counts collected during the period 2000–2016.

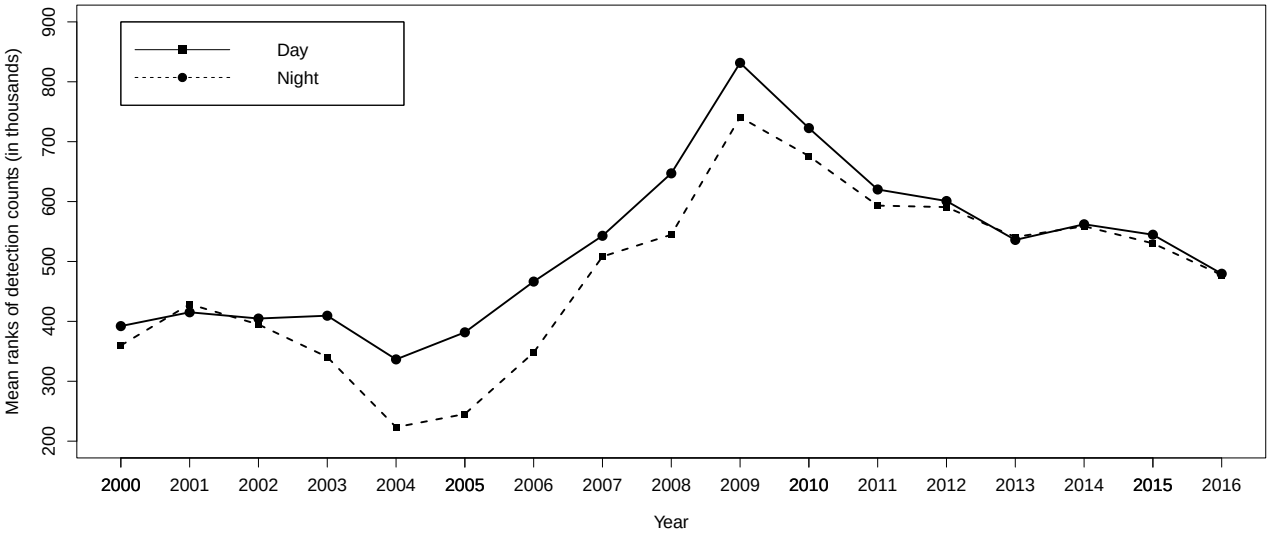

Figure 5 – Plot of mean ranks of day-time and night-time detection counts collected during the period 2000–2016.

groups of year detection counts. It was confirmed (in all cases $p < 0.001$) that detection counts in 2009–2010 are higher from other detection counts, and that detection counts for 2009 are the highest.

We will now test the hypothesis about the significance of the effects of period of the day and latitude class on detection counts. As the effect of year on detection counts is significant, we will perform analyses for each year separately, including a separate ranking of the data by year. The number and mean rank of detection counts by year, period of the day, and latitude class are given in Table 4. There is no year where all latitude classes are considered.

In the years 2005–2016 there were at least two latitude classes and the analyses of the effects of the period of the day and latitude class on detection counts could be performed. In 2004, although the N(45–60) class is available, the sample size is more than 100 times smaller than the N(30–45) class. For testing the hypothesis, we used the Brunner-Dette-Munk non-parametric two-way ANOVA. For all the years in that range, the interaction effect of period of the day and latitude class on detection counts is significant. As this interaction effect is not part of the research hypotheses and is difficult to interpret, we will not analyse it in more detail. Also, the effect of period of the day on detection counts is significant in years 2005–2010 and 2012–2015. In 2011 ($p = 0.367$) and 2016 ($p = 0.172$) no difference between day-time and night-time detection counts was found. Effect of latitude class on detection counts in years 2005–2016 is significant.

We will first compare day-time and night-time detection counts, and then detection counts in latitude classes. Multiple comparisons between a selection of two classes were performed using the Brunner-Munzel test. For the years 2012–2015 and for some pairs of the

Table 4 – Number N and mean rank $\overline{R}$ of detection counts by year, latitude class and the period of the day.

Year	Day-time				Latitude									
	Day		Night		S(30–45)		S(15–30)		N(15–30)		N(30–45)		N(45–60)	
	N	$\overline{R}$	N	$\overline{R}$	N	$\overline{R}$	N	$\overline{R}$	N	$\overline{R}$	N	$\overline{R}$	N	$\overline{R}$
2000	4 114	4 396.6	4 475	4 492.7	—	—	—	—	—	—	8 889	4 445.0	—	—
2001	4 112	4 323.7	4 229	4 022.6	—	—	—	—	—	—	8 341	4 171.0	—	—
2002	4 346	4 313.7	4 364	4 397.2	—	—	—	—	—	—	8 710	4 355.5	—	—
2003	3 915	3 560.7	3 904	4 260.3	—	—	—	—	—	—	7 819	3 910.0	—	—
2004	4 947	4 054.7	4 977	5 864.8	—	—	—	—	—	—	9 838	4 920.6	86	9 754.8
2005	2 832	2 333.4	2 931	3 412.0	—	—	—	—	—	—	5 612	2 814.9	151	5 377.1
2006	2 853	2 290.9	2 673	3 267.9	—	—	—	—	—	—	5 065	2 540.0	461	5 219.2
2007	2 268	1 888.3	1 710	2 123.8	—	—	—	—	—	—	2 475	1 269.5	1 503	3 175.1
2008	863	565.5	367	733.1	—	—	—	—	—	—	567	810.3	663	448.9
2009	14 658	11 287.7	10 392	14 271.5	—	—	—	—	—	—	3 217	3 422.2	21 833	13 866.8
2010	34 316	28 669.4	25 882	31 995.6	79	668.2	—	—	—	—	15 375	19 994.3	44 744	33 623.8
2011	41 921	35 154.6	30 064	37 162.1	1 041	3 717.6	—	—	24	31 224.2	23 103	31 688.1	47 817	38 778.0
2012	79 617	67 428.6	56 459	68 898.5	—	—	3 609	11 010.9	—	—	34 148	64 680.0	98 319	71 298.3
2013	97 633	85 896.8	73 516	85 147.7	—	—	4 514	13 291.8	4 631	72 606.7	52 246	75 750.8	109 758	93 771.4
2014	106 062	95 247.7	85 046	95 937.1	415	20 747.7	—	—	1 147	113 100.0	71 056	101 764.4	118 490	91 922.7
2015	106 107	95 817.0	87 831	98 361.9	6 123	105 943.3	84	60 377.1	—	—	56 192	92 753.7	131 539	98 376.1
2016	99 795	93 530.3	87 622	93 912.6	5 937	82 949.1	—	—	2 213	84 153.8	49 119	80 725.9	130 148	99 262.3

groups, Brunner-Munzel statistics could not be calculated. In these cases, the Wilcoxon sum rank test was used instead.

Mean ranks of day-time and night-time detection counts by year are represented in Figure 5. In most years, night-time detection counts are higher than day-time detection counts.

Results of the multiple comparisons between day-time and night-time detection counts are given in Table 5. By the formal statistical testing, it is confirmed that for 12 out of 17 years, night-time detection counts are higher than day-time detection counts.

We should note that, although the two-way ANOVA did not find any significant differences between day-time and night-time detection counts in 2011, further analyses (Brunner-Munzel test) showed that a difference probably exists ($p < 0.001$).

Mean ranks of detection counts in latitude classes by year are presented in Figure 6. The detection counts vary greatly in the same latitude class by year. In most years, detection counts in the N(45–60) class are higher than detection counts in the N(30–45) class.

Results of the formal testing of the differences between detection counts in latitude classes is given in Table 6. In the third column of the table are listed classes excluded from the multiple comparisons because of a sample size that is too small. The detection counts in the N(45–60) class are higher than detection counts in the N(30–45) class in 10 out of 12 years where both classes have large enough sample sizes.

4 Discussion

4.1 Effect of year on detection counts

The apparent maximum in detection counts between 2009–2010 is significant. This period is the same as the period of solar minimum (Figure 7). This correlation between solar minima and radio meteor detection counts maxima is noted in other articles (Lindblad, 1968).

That the solar cycle has an impact on meteor detection rates is not unexpected; the solar cycle heavily influences solar wind and electron line density in the upper atmosphere, and this has been known for some time (Wright, 1962). These changes in the ionosphere can have a large influence on detection rates, especially for radio meteor detection. It is necessary to ask whether the detection count maximum is a result of reduced noise, or an enhancement of radio signal intensities. No analysis of this is made.

Analysis of fit between an idealised diurnal shift curve and a given observer's data (Powell, 2017) suggests that the background detection rate increases between 2005 and 2011, but the intensity of diurnal shift does not, supporting the result that there is an increase in detection counts between 2009 and 2010. The density of debris surrounding Earth is likely not the cause of the detection count maximum, since this would also increase the intensity of diurnal shift. Rather, the noted maximum in detection counts must be due to better detecting conditions.

4.2 Effect of latitude on detection counts

Our results indicate (but do not fully confirm) that greater hourly detection counts are seen at greater latitudes. Whilst this appears to contradict Singer et al.

Table 5 – Relationship between day-time and night-time detection counts by year.

Relationship between day and night counts	Year
$day = night$	2000, 2002, 2016
$day > night$	2001, 2013
$day < night$	2003–2012, 2014–2015

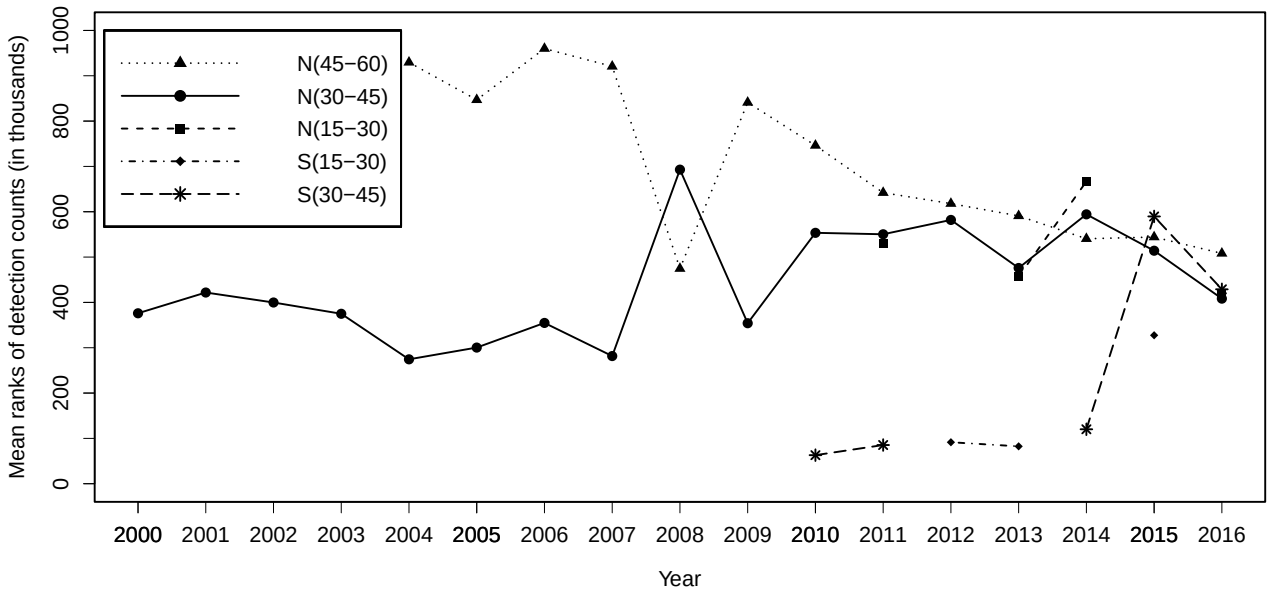

Figure 6 – Plot of mean ranks of detection counts in latitude classes collected during the period 2000–2016.

(2005), their research noted a relationship between diurnal rates and latitude, not overall detection rates as in our research. It is not clear why detection counts would be affected by latitude, nor why both latitude and period of the day interact to cause an effect.

A statistically significant difference in detection rates is found with class N(45–60) observing greater hourly detection counts than N(30–45) in 10 of 12 years. However, overall the relationship between latitude and detection counts is not clear.

4.3 Day-time and night-time rates

The fact that there is a statistically significant increase in detection rates during night-time could be due to many effects. A likely explanation is due to the change in ionospheric structure at night. With the absence of solar excitation, the ionisation of the D and E layers dramatically decreases, whilst the F layer remains well ionised, resulting in more free electrons, enabling radio signals to travel further — this was first reported in 1938 and is well studied (Booker & Wells, 1938). This effectively increases the area over which meteors can be detected, resulting in slightly higher detection rates. The effect is not large, since the increase in detection capability in the area of atmosphere where meteor burn-ups occur is little — it is largely an increase in range.

Theoretically, the peak hour of diurnal shift occurs at 6am, so any influence will be uniform between day and night (with the method of defining day or night as defined), and thus this phenomenon can be disregarded.

Table 6 – Relationship between detection counts in latitude classes by year.

Year	Relationship between latitude counts	Excluded latitude class
2005–2007, 2009	N(45–60)>N(30–45)	—
2008	N(45–60)<N(30–45)	—
2010	N(45–60)>N(30–45)	S(30–45)
2011	N(45–60)>N(30–45)>S(30–45)	N(15–30)
2012	N(45–60)>N(30–45)>S(15–30)	—
2013	N(45–60)>N(30–45)>N(15–30)>S(15–30)	—
2014	N(15–30)>N(30–45)>N(45–60)	S(30–45)
2015	S(30–45)>N(45–60)>N(30–45)	S(15–30)
2016	N(45–60)>N(15–30)>N(30–45)=S(30–45)	—

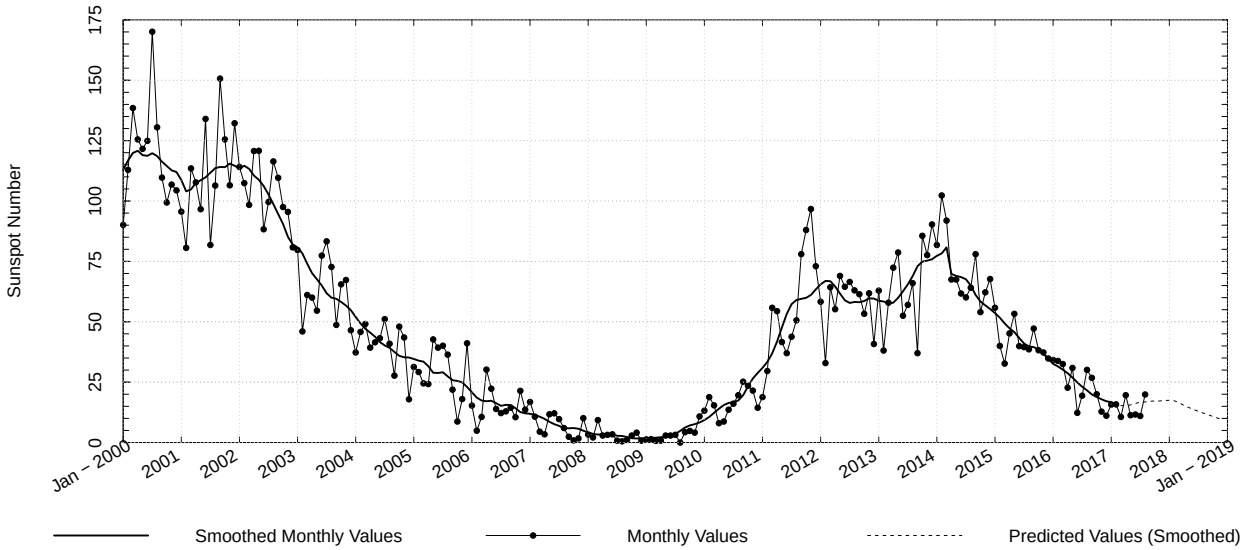

Figure 7 – Solar cycle sunspot number over time, observed data through 2017 August (Data provided by NOAA/SWPC (`http://www.swpc.noaa.gov`)).

There is a potential inaccuracy in the way day-time and night-time is defined for this analysis. Choosing night as a 12 hour period centred on local midnight allows analysis of the data whilst avoiding a large degree of complexity in calculating actual day and night for the observer. However, this simplification means that some items of data may be considered part of the day, but where recorded during the night. Overall this effect should be minimal, since the definition of day as 12 hours centred at midnight used can be viewed as an 'average' day across an entire year.

4.4 Annual scale variation

The increase in the middle of the year may be due to an increased number of meteor showers, or another phenomenon. This increase is likely due to an event or mechanism occurring during summer in the Northern Hemisphere, since most observers in the sample are in the Northern Hemisphere. The summer increase is in agreement with Singer et al. (2005).

The mid-year increase is likely not due to Earth's position relative to other bodies, which may sweep up meteors. The observed variation is an apparently annual occurrence, but Earth's position relative to other bodies is not periodic over the same period.

4.5 Monthly scale variation

It is unsurprising that there is no overall trend over the course of any month. Any variation on this scale could potentially (though unlikely to) be caused by the moon, though it is unlikely that it would have a significant impact, and this is seen in the results. The only clear increases in any month are the major meteor showers, namely the Perseids in August, Geminids in December, and Quadrantids in January.

4.6 Hemispheric effects

Specific northern and southern sources of meteors exist. Thus the temporal variations of hourly detection counts may be different between each hemisphere. However, variation over periods beyond a year are unlikely to be affected, since any difference between the hemispheres would counteract one another. Effects over shorter periods, such as sub-annually, may not counteract. Differences in sub-annual and sub-monthly variations should be considered in more scrutiny by hemisphere. Only 9 observers from the available data used for this analysis are in the Southern hemisphere, making any conclusions difficult to obtain. Therefore these effects have not been considered and are an important analysis to make in the future.

5 Conclusion

1. There is no clear variation in hourly detection counts over a month other than due to major meteor showers.

2. An increase in detection counts is observed during the summer months, with no clear explanation.

3. A statistically significant increase in hourly detection counts is present between 2009 and 2010.

4. The noted increase in meteor detection counts between 2009 and 2010 appears to correlate with a solar minimum, supporting hypotheses from Lindblad (1968) and Bumba (1949).

5. The effect of period of the day and latitude on detection counts is statistically significant.

6. For 12 out of 17 years between 2000 and 2016, night-time detection counts are greater than day-time detection counts, potentially due to changes in ionospheric structure between day and night.

7. In 10 out of 12 years tested between 2000 and 2016, observers in latitudes 45°–60° observe greater detection counts than observers in latitudes 30°–45°.

Acknowledgements

Permission for the use of data is kindly provided by the RMOB organisation. This work has in part been supported by the Norman Lockyer Observatory[b] and Exeter Mathematics School[c]. We are grateful to Michael Andrejczuk and Malcolm Simpson for their suggestions and advice.

References

Booker H. G. and Wells H. W. (1938). "Scattering of radio waves by the F-region of the ionosphere". *Journal of Geophysical Research*, **43:3**, 249–256.

Brunner E., Dette H., and Munk A. (1997). "Box-type approximations in non-parametric factorial designs". *Journal of the American Statistical Association*, **92**, 1494–1502.

Brunner E. and Munzel U. (2000). "The nonparametric Behrens-Fisher problem: asymptotic theory and a small-sample approximation". *Biometrical Journal*, **42**, 17–25.

Bumba V. (1949). "Influence de l'activité solaire sur le nombre des observations de météores, de traînées météoriques et de chutes météoriques". *Bulletin of the Astronomical Institutes of Czechoslovakia*, **1**, 93–95.

Conover W. J., Johnson M. E., and Johnson M. M. (1981). "A comparative study of tests for homogeneity of variances, with applications to the outer continental shelf bidding data". *Technometrics*, **23**, 351–361.

Lindblad B. A. (1968). "Long-term variations in meteor radar rates, meteor heights and radar-echo amplitudes". In Kresak L. and Millman P. M., editors, *Physics and Dynamics of Meteors*, volume 33 of *IAU Symposium*. pages 50–62.

Powell C. (2017). "Modelling and analysis of diurnal variation in meteor flux". *WGN, Journal of the IMO*, **45:2**, 32–37.

Singer W., von Zahn U., Batista P. P., Fuller B., and Latteck R. (2005). "Diurnal and annual variations of meteor rates at latitudes between 69°N and 35°S". In Warmbein B., editor, *17th ESA Symposium on European Rocket and Balloon Programmes and Related Research*, volume 590 of *ESA Special Publication*. pages 151–156.

Wilcox R. (2012). *Introduction to Robust Estimation and Hypothesis Testing, First Edition*. Elsevier.

Wilcox R. (2016). "R code". `http://dornsife.usc.edu/assets/sites/239/docs/Rallfun-v33.txt` .

Wright J. W. (1962). "Dependence of the ionospheric F region on the solar cycle [Letter to the editor]". *Nature*, **4827**, 461.

Handling Editor: Javor Kac
This paper has been typeset from a LaTeX file prepared by the authors.

[b] `http://www.normanlockyer.com`
[c] `https://www.exetermathematicsschool.ac.uk`

Preliminary results

Results of the IMO Video Meteor Network — February 2017

Sirko Molau[1], *Stefano Crivello*[2], *Rui Goncalves*[3], *Carlos Saraiva*[4], *Enrico Stomeo*[5], *and Javor Kac*[6]

The IMO Video Meteor Network cameras recorded more than 14 000 meteors in about 7 000 hours of observing time during 2017 February. The flux density profiles resulting from observations from 2012 to 2017 are presented for the following minor showers: α-Coronae Borealids, February ε-Virginids, February η-Draconids, π-Hydrids, β-Herculids, and February μ-Virginids. Most showers display a nearly constant activity, with the exception of the February η-Draconids which peak on February 2/3.

Received 2017 August 2

1 Introduction

Seventy-five video cameras contributed to the IMO Video Meteor Network in February 2017. They recorded about 14 000 meteors in 7 000 hours of effective observing time (Table 1 and Figure 1). The monthly statistics reveal large gaps and so the output was below the average of the last five years. This month's nightly flux ranged from less than a hundred meteors during the night of February 11/12 up to more than a thousand meteors per night in mid-February. With an average of 2.0 meteors per hour we were approaching the annual activity low.

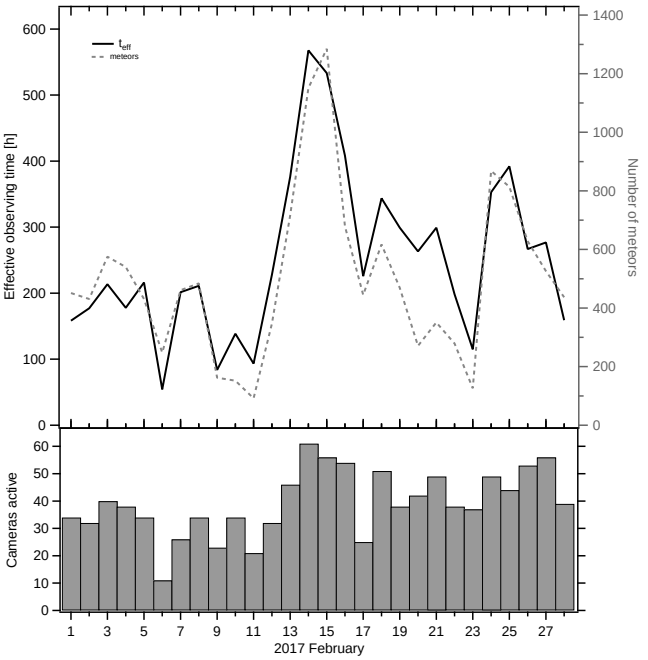

Figure 1 – Monthly summary for the effective observing time (solid black line), number of meteors (dashed gray line) and number of cameras active (bars) in 2017 February.

2 Minor showers of February

Since there are no noteworthy meteor showers in February, we focused on a set of minor showers close to the detection limit. Specifically, we analyzed six meteor showers in detail which we detected in the IMO Network data during our 2012/2013 analysis (Molau et al., 2013; Molau, 2014). What shape of activity profile would we see now that we have collected continuous flux density measurements over six years? The answer is revealed in the graphs which follow.

2.1 α-Coronae Borealids

The α-Coronae Borealids (429 ACB) are active across the January-February boundary. Overall, we recorded 1 500 shower members between January 26 and February 4 at an effective collection area of 830 000 km^2 per hour. For comparison: during the same period, we observed 9 000 sporadic and 3 000 Antihelion meteors. The mean profile (Figure 2) shows a constant level of activity with a flux density of 2 meteoroids per 1 000 km^2 per hour. The activity profiles of the individual years do not differ significantly from the average.

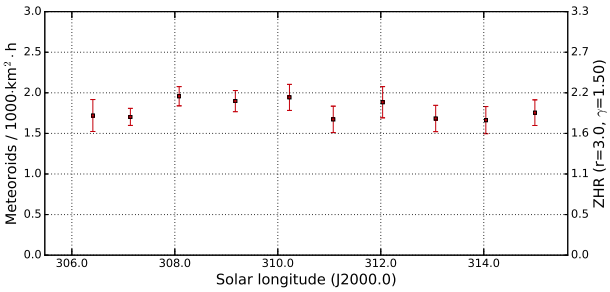

Figure 2 – Average flux density profile of the alpha Coronae Borealids in the years 2012 to 2017, derived from video data of the IMO Network.

[1]Abenstalstr. 13b, 84072 Seysdorf, Germany.
Email: sirko@molau.de
[2]Via Bobbio 9a/18, 16137 Genova, Italy.
Email: stefano.crivello@libero.it
[3]Urbanizacao da Boavista, Lote 46, Linhaceira, 2305-114 Asseiceira, Tomar, Portugal. Email: rui.goncalves@ipt.pt
[4]Rua Aquilino Ribeiro, 23 - 1 Dto. 2790028 Carnaxide, Portugal. Email: carlos.saraiva@netcabo.pt
[5]via Umbria 21/d, 30037 Scorze (VE), Italy.
Email: stom@iol.it
[6]Na Ajdov hrib 24, 2310 Slovenska Bistrica, Slovenia.
Email: javor.kac@orion-drustvo.si

IMO bibcode WGN-454-molau-vidfeb
NASA-ADS bibcode 2017JIMO...45...82M

2.2 February ε-Virginids

The activity period of the February ε-Virginids (506 FEV) lasts from January 28 to February 8. 1 700 shower members (12 000 SPO / 3 600 ANT) were recorded during this time with an effective collection area of more than 1.3 million km^2 per hour. Once again, we find a smooth activity profile without a clear peak (Figure 3), but the absolute flux density level is lower than before. The individual annual profiles do not provide additional information.

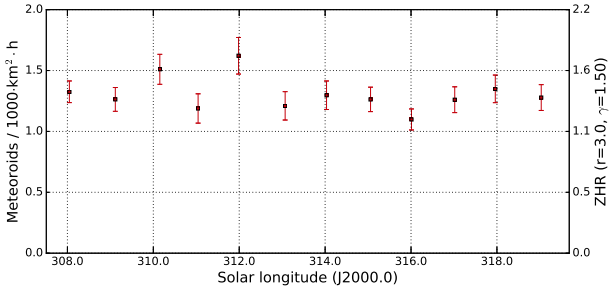

Figure 3 – Average flux density profile of the February ε-Virginids in the years 2012 to 2017, derived from video data of the IMO Network.

2.3 February η-Draconids

In parallel, but with a shorter activity window, we find the February η-Draconids (427 FED). The shower is detectable between February 2 and 5 and provides the smallest flux density of all the showers analyzed here, but it is the only one with a classical activity profile (Figure 4). Thanks to the circumpolar radiant we obtained a remarkable effective collection area of 880 000 km^2 per hour despite the short activity interval. Overall 400 shower members (4 000 SPO / 1 200 ANT) were recorded. Peak activity is reached at 315°.2 solar longitude (2017 February 3, at 02^{h}00^m UT). A look at the individual years reveals that the 2013 peak was particularly prominent.

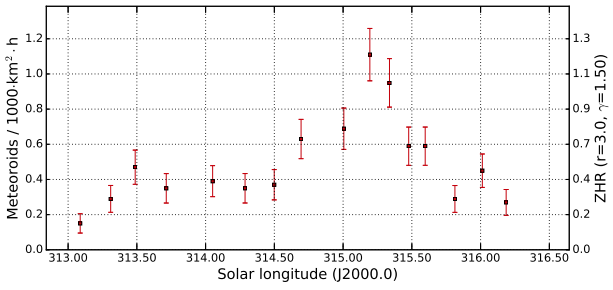

Figure 4 – Average flux density profile of the February η-Draconids in the years 2012 to 2017, derived from video data of the IMO Network.

2.4 π-Hydrids

The minor shower of the π-Hydrids (101 PIH) is active between February 3 and 9. Despite the effective collection area of only 180 000 km^2 per hour we assigned 650 meteors to that radiant (7 000 SPO / 2 100 ANT). Indeed, the flux density reaches larger values of almost 4 meteoroids per 1 000 km^2 per hour. There are no outliers in the individual years.

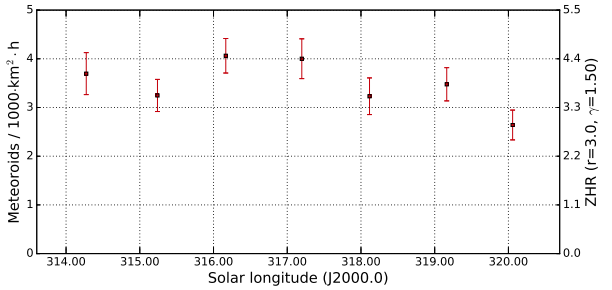

Figure 5 – Average flux density profile of the π-Hydrids in the years 2012 to 2017, derived from video data of the IMO Network.

2.5 β-Herculids

In the middle of February, we find the β-Herculids (418 BHE). Between February 12 and 16 we recorded 700 shower members (5 000 SPO / 1 700 ANT) with an effective collection area of 700 000 km^2 per hour. The flux density level is constant at a level of 1 meteoroid per 1 000 km^2 per hour (Figure 6) and there are no significant deviations in individual years.

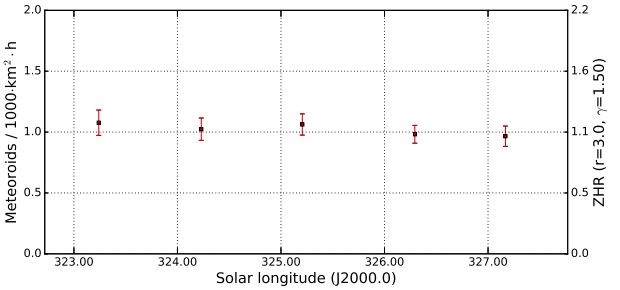

Figure 6 – Average flux density profile of the β-Herculids in the years 2012 to 2017, derived from video data of the IMO Network.

2.6 February μ-Virginids

Last but not least we obtained data from 2 000 February μ-Virginids (516 FMV) from February 14 to 28 (14 000 SPO / 4 800 ANT). The collection area of the IMO Network totalled nearly a million km^2 per hour. The activity profile shows only small variations as in the earlier cases (Figure 7) and the flux density scatters around a value of 2 meteoroids per 1 000 km^2 per hour.

Looking at the profiles of the individual years we find indeed an outlier on 2014 February 18/19, for which the flux density was by a factor 4 to 5 higher than usual (Figure 8). Looking in more detail, this peak is made up of ten shower members which were recorded during a night with a particularly small effective collection area. In fact, we can even further pin down the outlier to

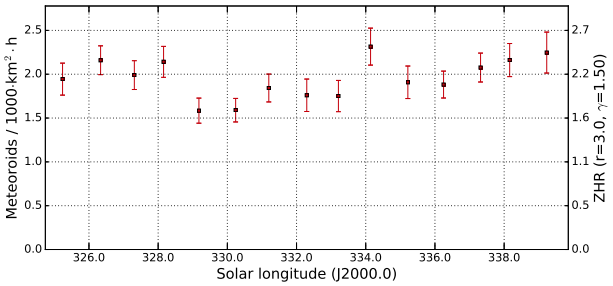

Figure 7 – Average flux density profile of the February μ-Virginids in the years 2012 to 2017, derived from video data of the IMO Network.

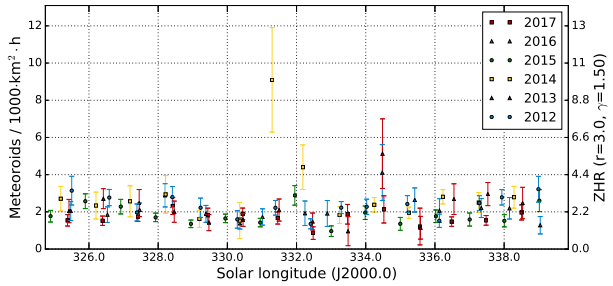

Figure 8 – Individual profiles of the February μ-Virginids in the years 2012 to 2017.

five shower meteors recorded by all active video network cameras between 02^{h} and 04^{h} UT. Hence we can assume that this outlier is of statistical nature only.

3 Summary

In summary we can conclude that no February source stands clearly out of the background. Only the February η-Draconids provide a classical activity profile with a peak on February 2/3. In this case, our video cameras are particularly effective data collectors thanks to the favorable location of the radiant and the low meteor shower velocity.

References

Molau S. (2014). "Meteor showers identified from one million video meteors". In Gyssens M., Roggemans P., and Zoladek P., editors, *Proceedings of the International Meteor Conference, Poznan, Poland, 22-25 August 2013*. pages 26–38.

Molau S., Kac J., Berko E., Crivello S., Stomeo E., Igaz A., Barentsen G., and Goncalves R. (2013). "Results of the IMO Video Meteor Network – February 2013". *WGN, Journal of the IMO*, **41:3**, 92–95.

Handling Editor: Javor Kac

Code	Name	Location	Camera	FOV [°²]	Stellar LM [mag]	Eff.CA [km²]	Nights	Time [h]	Meteors
ARLRA	Arlt	Ludwigsfelde/DE	Ludwig2 (0.8/8)	1475	6.2	3779	17	85.9	327
BOMMA	Bombardini	Faenza/IT	Mario (1.2/4.0)	5794	3.3	739	17	102.8	268
BREMA	Breukers	Hengelo/NL	Mbb3 (0.75/6)	2399	4.2	699	11	77.2	108
BRIBE	Klemt	Herne/DE	Hermine (0.8/6)	2374	4.2	678	14	87.8	151
		Bergisch Gladbach/DE	Klemoi (0.8/6)	2286	4.6	1080	15	84.0	132
CARMA	Carli	Monte Baldo/IT	Bmh2 (1.5/4.5)*	4243	3.0	371	16	124.9	449
CINFR	Cineglosso	Faenza/IT	Jenni (1.2/4)	5886	3.9	1222	16	98.7	288
CRIST	Crivello	Valbrevenna/IT	Bilbo (0.8/3.8)	5458	4.2	1772	14	89.7	175
			C3P8 (0.8/3.8)	5455	4.2	1586	14	90.9	351
			Stg38 (0.8/3.8)	5614	4.4	2007	16	111.1	168
ELTMA	Eltri	Venezia/IT	Met38 (0.8/3.8)	5631	4.3	2151	12	72.0	111
FORKE	Förster	Carlsfeld/DE	Akm3 (0.75/6)	2375	5.1	2154	11	81.3	150
GONRU	Goncalves	Foz do Arelho/PT	Farelho1 (1.0/2.6)	6328	2.8	469	6	7.7	23
		Tomar/PT	Templar1 (0.8/6)	2179	5.3	1842	23	173.1	373
			Templar2 (0.8/6)	2080	5.0	1508	23	163.9	277
			Templar3 (0.8/8)	1438	4.3	571	19	144.6	121
			Templar4 (0.8/3.8)	4475	3.0	442	23	153.7	287
			Templar5 (0.75/6)	2312	5.0	2259	22	141.2	260
GOVMI	Govedič	Središče ob Dravi/SI	Orion2 (0.8/8)	1447	5.5	1841	18	117.3	138
			Orion4 (0.95/5)	2662	4.3	1043	12	86.4	85
HERCA	Hergenrother	Tucson/US	Salsa3 (0.8/3.8)	2336	4.1	544	25	216.3	338
HINWO	Hinz	Schwarzenberg/DE	Hinwo1 (0.75/6)	2291	5.1	1819	15	90.8	165
IGAAN	Igaz	Hódmezővásárhely/HU	Huhod (0.8/3.8)	5502	3.4	764	13	77.1	58
		Budapest/HU	Hupol (1.2/4)	3790	3.3	475	10	57.6	27
JONKA	Jonas	Budapest/HU	Husor (0.95/4)	2286	3.9	445	11	42.9	51
			Husor2 (0.95/3.5)	2465	3.9	715	12	52.6	44
KACJA	Kac	Ljubljana/SI	Orion1 (0.8/8)	1399	3.8	268	9	48.9	28
		Kamnik/SI	Cvetka (0.8/3.8)*	4914	4.3	1842	7	53.0	131
			Rezika (0.8/6)	2270	4.4	840	8	58.0	237
			Stefka (0.8/3.8)	5471	2.8	379	6	49.9	77
		Kostanjevec/SI	Metka (0.8/12)*	715	6.4	640	16	100.3	111
KOSDE	Koschny	Izana Obs./ES	Icc7 (0.85/25)*	714	5.9	1464	12	72.3	368
			Lic1 (2.8/50)*	2255	6.2	5670	14	119.5	736
		La Palma/ES	Icc9 (0.85/25)*	683	6.7	2951	14	119.1	736
LOJTO	Łojek	Grabniak/PL	Pav57 (1.0/5)	1631	3.5	269	9	60.5	81
LOPAL	Lopes	Lisbon/PT	Naso1 (0.75/6)	2377	3.8	506	18	95.2	82

Table 1 – Observers contributing to 2017 February data of the IMO Video Meteor Network. Eff.CA designates the effective collection area; the overall number of nights is the number of nights with at least one camera operating, the overall observing time and number of meteors are sums over all cameras.

Table 1 – Observers contributing to 2017 February data of the IMO Video Meteor Network – continued from previous page.

Code	Name	Location	Camera	FOV [°²]	Stellar LM [mag]	Eff.CA [km²]	Nights	Time [h]	Meteors
MACMA	Maciejewski	Chełm/PL	Pav35 (0.8/3.8)	5495	4.0	1584	14	67.2	70
			Pav36 (0.8/3.8)*	5668	4.0	1573	11	60.7	49
			Pav43 (0.75/4.5)*	3132	3.1	319	13	60.2	55
			Pav60 (0.75/4.5)	2250	3.1	281	11	64.3	99
MARRU	Marques	Lisbon/PT	Cab1 (0.75/6)	2362	4.8	1517	22	166.0	262
			Ran1 (1.4/4.5)	4405	4.0	1241	16	137.1	156
MASMI	Maslov	Novosibirsk/RU	Nowatec (0.8/3.8)	5574	3.6	773	4	17.2	31
MOLSI	Molau	Seysdorf/DE	Avis2 (1.4/50)*	1230	6.9	6152	21	119.6	550
			Escimo2 (0.85/25)	155	8.1	3415	16	121.6	220
			Mincam1 (0.8/8)	1477	4.9	1084	18	109.4	281
		Ketzür/DE	Remo1 (0.8/8)	1467	6.5	5491	18	89.1	290
			Remo2 (0.8/8)	1478	6.4	4778	19	102.3	366
			Remo3 (0.8/8)	1420	5.6	1967	16	98.9	177
			Remo4 (0.8/8)	1478	6.5	5358	18	96.7	310
MORJO	Morvai	Fülöpszállás/HU	Huful (1.4/5)	2522	3.5	532	12	89.4	68
OTTMI	Otte	Pearl City/US	Orie1 (1.4/5.7)	3837	3.8	460	21	138.1	180
PERZS	Perkó	Becsehely/HU	Hubec (0.8/3.8)*	5498	2.9	460	20	141.3	274
ROTEC	Rothenberg	Berlin/DE	Armefa (0.8/6)	2366	4.5	911	6	34.1	27
SARAN	Saraiva	Carnaxide/PT	Ro1 (0.75/6)	2362	3.7	381	19	135.2	141
			Ro2 (0.75/6)	2381	3.8	459	21	142.8	191
			Ro3 (0.8/12)	710	5.2	619	21	131.1	224
			Ro4 (1.0/8)	1582	4.2	549	18	82.2	80
			Sofia (0.8/12)	738	5.3	907	16	110.3	102
SCALE	Scarpa	Alberoni/IT	Leo (1.2/4.5)*	4152	4.5	2052	12	69.0	69
SCHHA	Schremmer	Niederkrüchten/DE	Doraemon (0.8/3.8)	4900	3.0	409	15	100.2	179
SLAST	Slavec	Ljubljana/SI	Kayak1 (1.8/28)	563	6.2	1294	2	10.9	28
			Kayak2 (0.8/12)	741	5.5	920	2	16.6	5
STOEN	Stomeo	Scorze/IT	Min38 (0.8/3.8)	5566	4.8	3270	15	90.6	255
			Noa38 (0.8/3.8)	5609	4.2	1911	15	100.8	252
			Sco38 (0.8/3.8)	5598	4.8	3306	13	66.0	221
STRJO	Strunk	Herford/DE	Mincam2 (0.8/6)	2354	5.4	2751	15	88.3	230
			Mincam3 (0.8/6)	2338	5.5	3590	16	85.2	126
			Mincam5 (0.8/6)	2349	5.0	1896	14	90.8	149
			Mincam6 (0.8/6)	2395	5.1	2178	15	85.7	111
TEPIS	Tepliczky	Agostyán/HU	Huago (0.75/4.5)	2427	4.4	1036	16	106.2	91
			Humob (0.8/6)	2388	4.8	1607	18	117.6	146
WEGWA	Wegrzyk	Nieznaszyn/PL	Pav78 (0.8/6)	2286	4.0	778	12	72.6	80
YRJIL	Yrjölä	Kuusankoski/FI	Finexcam (0.8/6)	2337	5.5	3574	12	87.0	127
* active field of view smaller than video frame						Overall	28	7 030.3	14 036

Results of the IMO Video Meteor Network — March 2017

Sirko Molau[1], *Stefano Crivello*[2], *Rui Goncalves*[3], *Carlos Saraiva*[4], *Enrico Stomeo*[5], *and Javor Kac*[6]

In 2017 March, cameras of the IMO Video Meteor Network cameras recorded more than 18 000 meteors in over 10 000 hours of observing time. In the absence of any significant meteor showers in this month, the flux density profiles and population index profiles of the Antihelion meteors are compared to sporadics, using March observations from 2012 to 2017.

Received 2017 September 15

1 Introduction

In the last few years, the observers enjoyed favorable observing conditions in March, and 2017 was no exception. 47 out of 75 cameras that joined the IMO Network in this month, collected twenty or more observing nights. Even our Slovenian observers, who are often hampered by poor weather, experienced perfect observing conditions and collected up to 31 observing nights.

The overall effective observing time was slightly above 10 000 hours (Table 1 and Figure 1) and thereby above the average of the previous years. The mean of 1.8 meteors per hour is one of the smallest values we ever recorded – only March 2014 and 2015 were below this year's result with an average of 1.7 meteors per hour.

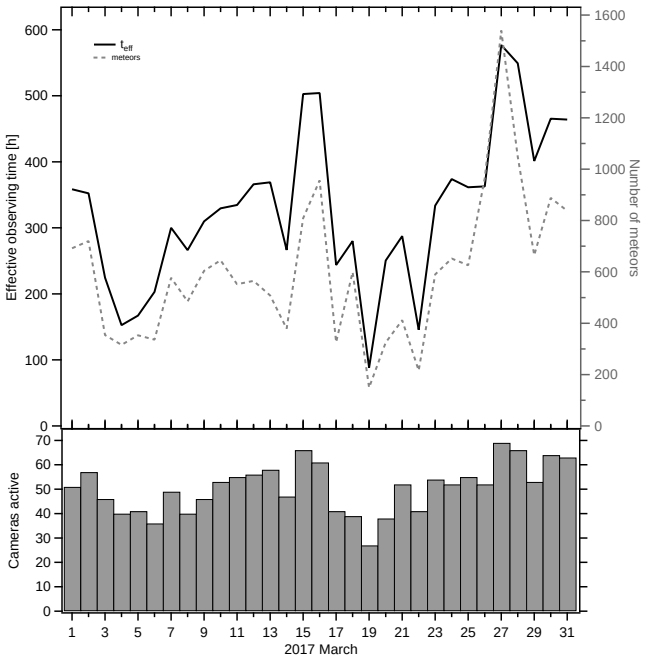

Figure 1 – Monthly summary for the effective observing time (solid black line), number of meteors (dashed gray line) and number of cameras active (bars) in 2017 March.

2 Antihelion meteors in March

In the absence of significant meteor showers, we had a quick look at the flux density of the Antihelion source (ANT) and sporadic meteors (SPO). Figure 2 compares the activity of both sources in the course of the month, whereby ANT (lighter/green, right axis) were one order of magnitude weaker than SPO (darker/red, left axis). Note that the Antihelion source is about twice as active in the middle of March compared to begin and end (whereby we omitted an outlier on March 19/20 caused by insufficient data), whereas sporadic activity is almost constant. After all, the Antihelion source is in reality a collection of smaller "streamlets" which are difficult to separate from one another. Hence, the increased activity at mid-March could be related to such a "streamlet".

It was not possible to obtain reliable r-values from the 2017 March data alone, because there were too few Anthelion meteors. However, we may average the population index over the last six years which has the additional advantage that lunar phase-dependent fluctuations are smeared out.

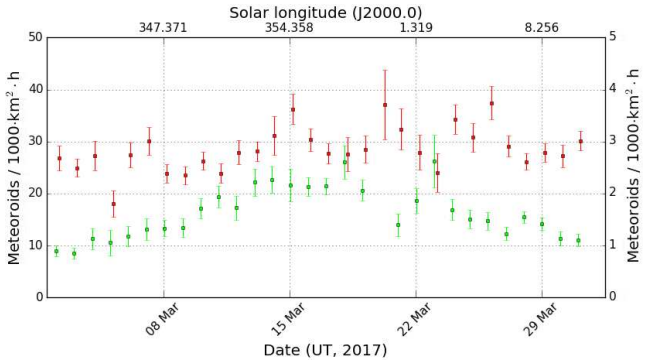

Figure 2 – Flux density profile of the Antihelion source (lighter/green, right axis) and sporadic meteors (darker/red, left axis) in 2017 March, derived from video data of the IMO Network.

Figure 3 shows for sporadic meteors (darker/red) an almost constant population index of about 2.7 with only minor scatter. Due to the smaller number of meteors, the scatter and error bars are bigger in case of the Antihelion source, but otherwise there are no systematic

[1]Abenstalstr. 13b, 84072 Seysdorf, Germany.
Email: sirko@molau.de
[2]Via Bobbio 9a/18, 16137 Genova, Italy.
Email: stefano.crivello@libero.it
[3]Urbanizacao da Boavista, Lote 46, Linhaceira, 2305-114 Asseiceira, Tomar, Portugal. Email: rui.goncalves@ipt.pt
[4]Rua Aquilino Ribeiro, 23 - 1 Dto. 2790028 Carnaxide, Portugal. Email: carlos.saraiva@netcabo.pt
[5]via Umbria 21/d, 30037 Scorze (VE), Italy.
Email: stom@iol.it
[6]Na Ajdov hrib 24, 2310 Slovenska Bistrica, Slovenia.
Email: javor.kac@orion-drustvo.si

IMO bibcode WGN-454-molau-vidmar
NASA-ADS bibcode 2017JIMO...45...87M

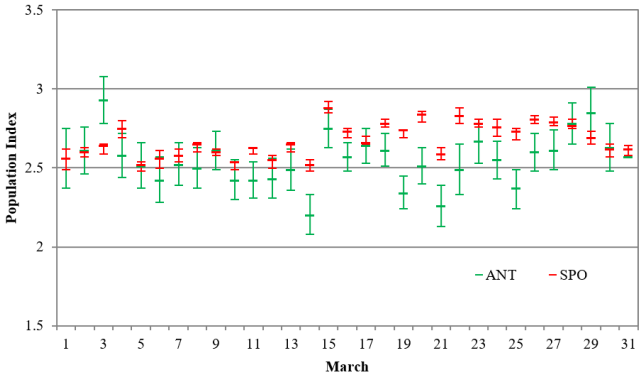

Figure 3 – Average population index of the Antihelion source (lighter/green) and sporadic meteors (darker/red) in March of 2012–2017, derived from video data of the IMO Network.

variations. The average is only 0.1 smaller than in case of sporadic meteors, i.e. the brightness distributions deviate only marginally from one another.

Handling Editor: Javor Kac

– Sporadic meteor lasting 3.2 s, recorded on 2015 March 5, $02^{h}50^{m}20^{s}$ UT by GONRU with Templar5.

– End of sporadic fireball with a clear segmentation in the end, captured on 2017 March 5, $22^{h}50^{m}11^{s}$ UT by PERSZ with Hubec.

– Sporadic with flickering, scenic view with Moon, clouds and landscape, captured on 2015 March 29, $21^{h}32^{m}22^{s}$ UT by GONRU with Templar4.

– Sporadic meteor that lasted for 5.2 s with an interesting light curve, recorded on 2017 April 1, $03^{h}34^{m}46^{s}$ UT by HINWO with Hinwo1.

Code	Name	Location	Camera	FOV [°²]	Stellar LM [mag]	Eff.CA [km²]	Nights	Time [h]	Meteors
ARLRA	Arlt	Ludwigsfelde/DE	Ludwig2 (0.8/8)	1475	6.2	3779	23	129.8	459
BERER	Berkó	Ludányhalászi/HU	Hulud1 (0.8/3.8)	5542	4.8	3847	13	97.4	249
BOMMA	Bombardini	Faenza/IT	Mario (1.2/4.0)	5794	3.3	739	29	204.6	484
BREMA	Breukers	Hengelo/NL	Mbb3 (0.75/6)	2399	4.2	699	22	126.2	162
BRIBE	Klemt	Herne/DE	Hermine (0.8/6)	2374	4.2	678	19	132.4	203
		Bergisch Gladbach/DE	Klemoi (0.8/6)	2286	4.6	1080	22	135.0	201
CARMA	Carli	Monte Baldo/IT	Bmh2 (1.5/4.5)*	4243	3.0	371	10	61.6	200
CASFL	Castellani	Monte Baldo/IT	Bmh1 (0.8/6)	2350	5.0	1611	22	187.2	328
CINFR	Cineglosso	Faenza/IT	Jenni (1.2/4)	5886	3.9	1222	22	168.0	243
CRIST	Crivello	Valbrevenna/IT	Bilbo (0.8/3.8)	5458	4.2	1772	26	188.6	376
			C3P8 (0.8/3.8)	5455	4.2	1586	22	173.0	224
			Stg38 (0.8/3.8)	5614	4.4	2007	28	217.6	566
ELTMA	Eltri	Venezia/IT	Met38 (0.8/3.8)	5631	4.3	2151	19	127.2	182
FORKE	Förster	Carlsfeld/DE	Akm3 (0.75/6)	2375	5.1	2154	17	100.8	217
GONRU	Goncalves	Foz do Arelho/PT	Farelho1 (1.0/2.6)	6328	2.8	469	25	72.9	98
		Tomar/PT	Templar1 (0.8/6)	2179	5.3	1842	28	194.6	354
			Templar2 (0.8/6)	2080	5.0	1508	28	185.8	291
			Templar3 (0.8/8)	1438	4.3	571	24	166.8	115
			Templar4 (0.8/3.8)	4475	3.0	442	27	162.4	282
			Templar5 (0.75/6)	2312	5.0	2259	27	156.9	230
GOVMI	Govedič	Središče ob Dravi/SI	Orion2 (0.8/8)	1447	5.5	1841	31	194.4	243
			Orion4 (0.95/5)	2662	4.3	1043	22	135.3	129
HERCA	Hergenrother	Tucson/US	Salsa3 (0.8/3.8)	2336	4.1	544	30	290.8	390
HINWO	Hinz	Schwarzenberg/DE	Hinwo1 (0.75/6)	2291	5.1	1819	17	119.4	173
IGAAN	Igaz	Hódmezővásárhely/HU	Huhod (0.8/3.8)	5502	3.4	764	18	109.9	83
		Budapest/HU	Hupol (1.2/4)	3790	3.3	475	14	82.7	42
JONKA	Jonas	Budapest/HU	Husor (0.95/4)	2286	3.9	445	20	105.5	108
			Husor2 (0.95/3.5)	2465	3.9	715	23	151.8	124
KACJA	Kac	Ljubljana/SI	Orion1 (0.8/8)	1399	3.8	268	26	185.4	331
		Kamnik/SI	Cvetka (0.8/3.8)*	4914	4.3	1842	17	145.7	332
			Rezika (0.8/6)	2270	4.4	840	18	146.0	535
			Stefka (0.8/3.8)	5471	2.8	379	17	139.9	228
		Kostanjevec/SI	Metka (0.8/12)*	715	6.4	640	27	194.2	183
KOSDE	Koschny	Izana Obs./ES	Icc7 (0.85/25)*	714	5.9	1464	5	35.4	169
			Lic1 (2.8/50)*	2255	6.2	5670	6	41.4	210
		La Palma/ES	Icc9 (0.85/25)*	683	6.7	2951	25	157.1	768
LOJTO	Łojek	Grabniak/PL	Pav57 (1.0/5)	1631	3.5	269	9	52.7	129
LOPAL	Lopes	Lisbon/PT	Naso1 (0.75/6)	2377	3.8	506	17	76.0	68

Table 1 – Observers contributing to 2017 March data of the IMO Video Meteor Network. Eff.CA designates the effective collection area; the overall number of nights is the number of nights with at least one camera operating, the overall observing time and number of meteors are sums over all cameras.

Table 1 – Observers contributing to 2017 March data of the IMO Video Meteor Network – continued from previous page.

Code	Name	Location	Camera	FOV [°²]	Stellar LM [mag]	Eff.CA [km²]	Nights	Time [h]	Meteors
MACMA	Maciejewski	Chełm/PL	Pav35 (0.8/3.8)	5495	4.0	1584	18	75.1	88
			Pav36 (0.8/3.8)*	5668	4.0	1573	19	99.7	116
			Pav43 (0.75/4.5)*	3132	3.1	319	16	96.0	85
			Pav60 (0.75/4.5)	2250	3.1	281	22	122.1	212
MARRU	Marques	Lisbon/PT	Cab1 (0.75/6)	2362	4.8	1517	26	199.1	274
			Ran1 (1.4/4.5)	4405	4.0	1241	20	129.5	161
MASMI	Maslov	Novosibirsk/RU	Nowatec (0.8/3.8)	5574	3.6	773	5	32.4	65
MOLSI	Molau	Seysdorf/DE	Avis2 (1.4/50)*	1230	6.9	6152	25	163.8	745
			Escimo2 (0.85/25)	155	8.1	3415	23	169.4	306
			Mincam1 (0.8/8)	1477	4.9	1084	23	155.9	421
		Ketzür/DE	Remo1 (0.8/8)	1467	6.5	5491	24	135.5	444
			Remo2 (0.8/8)	1478	6.4	4778	22	147.3	509
			Remo3 (0.8/8)	1420	5.6	1967	23	167.1	430
			Remo4 (0.8/8)	1478	6.5	5358	23	156.4	566
MORJO	Morvai	Fülöpszállás/HU	Huful (1.4/5)	2522	3.5	532	25	149.6	118
OTTMI	Otte	Pearl City/US	Orie1 (1.4/5.7)	3837	3.8	460	17	97.0	104
PERZS	Perkó	Becsehely/HU	Hubec (0.8/3.8)*	5498	2.9	460	29	199.2	346
ROTEC	Rothenberg	Berlin/DE	Armefa (0.8/6)	2366	4.5	911	6	37.3	51
SARAN	Saraiva	Carnaxide/PT	Ro1 (0.75/6)	2362	3.7	381	21	137.1	151
			Ro2 (0.75/6)	2381	3.8	459	18	116.1	149
			Ro3 (0.8/12)	710	5.2	619	20	109.2	205
			Ro4 (1.0/8)	1582	4.2	549	18	86.3	82
			Sofia (0.8/12)	738	5.3	907	23	121.5	134
SCALE	Scarpa	Alberoni/IT	Leo (1.2/4.5)*	4152	4.5	2052	24	122.8	116
SCHHA	Schremmer	Niederkrüchten/DE	Doraemon (0.8/3.8)	4900	3.0	409	24	156.3	199
SLAST	Slavec	Ljubljana/SI	Kayak2 (0.8/12)	741	5.5	920	24	191.3	104
STOEN	Stomeo	Scorze/IT	Min38 (0.8/3.8)	5566	4.8	3270	29	171.4	489
			Noa38 (0.8/3.8)	5609	4.2	1911	28	181.4	455
			Sco38 (0.8/3.8)	5598	4.8	3306	30	194.4	636
STRJO	Strunk	Herford/DE	Mincam2 (0.8/6)	2354	5.4	2751	21	110.7	265
			Mincam3 (0.8/6)	2338	5.5	3590	20	113.4	157
			Mincam5 (0.8/6)	2349	5.0	1896	15	95.9	120
			Mincam6 (0.8/6)	2395	5.1	2178	19	102.1	129
TEPIS	Tepliczky	Agostyán/HU	Huago (0.75/4.5)	2427	4.4	1036	14	106.8	95
			Humob (0.8/6)	2388	4.8	1607	24	176.0	198
WEGWA	Wegrzyk	Nieznaszyn/PL	Pav78 (0.8/6)	2286	4.0	778	19	103.1	119
YRJIL	Yrjölä	Kuusankoski/FI	Finexcam (0.8/6)	2337	5.5	3574	16	109.5	170
* active field of view smaller than video frame						Overall	31	10 190.1	18 723

The International Meteor Organization

www.imo.net

Follow us on Facebook InternationalMeteorOrganization

Follow us on Twitter @IMOMeteors

Council

President: Cis Verbeeck,
Bogaertsheide 5, 2560 Kessel, Belgium.
e-mail: cis.verbeeck@scarlet.be

Vice-President: Jürgen Rendtel,
Eschenweg 16, D-14476 Marquardt, Germany.
tel. +49 33208 50753
e-mail: jrendtel@aip.de

Secretary-General: Robert Lunsford,
14884 Quail Valley Way, El Cajon,
CA 92021-2227, USA. tel. +1 619 755 7791
e-mail: lunro.imo.usa@cox.net

Treasurer: Marc Gyssens, Heerbaan 74,
B-2530 Boechout, Belgium.
e-mail: marc.gyssens@uhasselt.be
BIC: GEBABEBB
IBAN: BE30 0014 7327 5911
Bank transfer costs are always at your expense.

Other Council members:

Megan Argo, Jodrell Bank Centre for Astrophysics, Alan Turing building, University of Manchester, Oxford Road, Manchester, M13 9PL, UK.
e-mail: megan.argo@gmail.com

Geert Barentsen, NASA Ames Research Center, M/S 244-30, Moffett Field CA 94035, USA.
e-mail: hello@geert.io

Javor Kac (see details under WGN)

Detlef Koschny, Zeestraat 46,
NL-2211 XH Noordwijkerhout, Netherlands.
e-mail: detlef.koschny@esa.int

Masahiro Koseki, 4-3-5 Annaka, Annaka-shi,
Gunma-ken 379-0116, Japan.
e-mail: geh04301@nifty.ne.jp

Sirko Molau, Abenstalstraße 13b, D-84072 Seysdorf, Germany. e-mail: sirko@molau.de

Jean-Louis Rault, Société Astronomique de France, 16, rue de la Vallée, 91360 Epinay sur Orge, France. e-mail: f6agr@orange.fr

Paul Roggemans, Pijnboomstraat 25, 2800 Mechelen, Belgium, e-mail: paul.roggemans@gmail.com

Galina Ryabova, Res. Inst. of Appl. Math. & Mech., Tomsk State University, Lenin pr. 36, build. 27, 634050 Tomsk, Russian Federation.
e-mail: ryabova@niipmm.tsu.ru

Damir Šegon, J. Rakovca 3, 52100 Pula, Croatia. e-mail: damir.segon@pu.t-com.hr

Juraj Tóth, Fac. Math., Phys. & Inf., Comenius Univ., Mlynska dolina, 84248 Bratislava, Slovakia.
e-mail: toth@fmph.uniba.sk

Commission Directors

Visual Commission: Rainer Arlt (rarlt@aip.de)
Generic e-mail address: visual@imo.net
Electronic visual report form:
http://www.imo.net/visual/report/electronic

Video Commission: Sirko Molau (video@imo.net)

Photographic Commission: Bill Ward (William.Ward@glasgow.ac.uk)
Generic e-mail address: photo@imo.net

Radio Commission: Jean-Louis Rault (radio@imo.net)

Fireballs: Online fireball reports:
http://fireballs.imo.net

Outreach Officer

Jure Atanackov, e-mail: jureatanackov@gmail.com

Press Officer

Megan Argo, e-mail: megan.argo@gmail.com

Webmaster

Karl Antier, e-mail: webmaster@imo.net

WGN

Editor-in-chief: Javor Kac
Na Ajdov hrib 24, SI-2310 Slovenska Bistrica, Slovenia. e-mail: wgn@imo.net;
include METEOR in the e-mail subject line

Editorial board: Ž. Andreić, M. Argo, D.J. Asher, F. Bettonvil, J. Correira, M. Gyssens, C. Hergenrother, T. Heywood, J. Rendtel, J.-L. Rault, C. Verbeeck, D. Vida, S. de Vet.

IMO Sales

Available from the Treasurer or the Electronic Shop on the IMO Website	€	$
IMO membership, including subscription to WGN Vol. 45 (2017)		
Surface mail	26	35
Air Mail (outside Europe only)	49	65
Electronic subscription only	21	25
Proceedings of the International Meteor Conference on paper		
1990, 1991, 1993, 1995, 1996, 1999, 2000, 2002, 2003, per year	9	12
2007, 2010, 2011, per year	15	20
2012, 2013, 2014, 2015 per year	25	34
2016	30	40
Proceedings of the Meteor Orbit Determination Workshop 2006	15	20
Radio Meteor School Proceedings 2005	15	20
Handbook for Meteor Observers	15	20
Meteor Shower Workbook	12	16
Electronic media		
Meteor Beliefs Project ZIP archive	6	8

Eta Aquariid fireball train on 2017 May 6

Evolution of the persistent train of the Eta Aquariid fireball that was imaged from Mount Bromo, Indonesia on 2017 May 6 at around $04^{\mathrm{h}}16^{\mathrm{m}}$ AM local time. The photograph showing the fireball is presented on the front cover.